Biomechanical Evaluation of an Optical System for Quantitative Human Motion Analysis

Jeffrey D. Kertis
Marquette University

BIOMECHANICAL EVALUATION OF AN OPTICAL SYSTEM FOR QUANTITATIVE HUMAN MOTION ANALYSIS

By

Jeffrey D. Kertis, B.S.

A Thesis Submitted to the Faculty of the Graduate School,
Marquette University,
in Partial Fulfillment of the Requirements for
the Degree of Master of Science

Milwaukee, Wisconsin

December 2012

ABSTRACT
BIOMECHANICAL EVALUATION OF AN OPTICAL SYSTEM
FOR QUANTITATIVE HUMAN MOTION ANALYSIS

Jeffrey D. Kertis, B.S.

Marquette University, 2012

An eight-camera Optitrack motion capture system was evaluated by performing static, linear dynamic, and angular dynamic calibrations using marker distances associated with upper and lower extremity gait and wheelchair models. Data were analyzed to determine accuracy and resolution within a defined capture volume using a standard Cartesian reference system. Two additional cameras along with AMASS and Visual3D (C-Motion, Inc., Germantown, MD) biomechanical modeling software were used to determine joint kinematics at the pelvis, hip, knee, and ankle of ten control subjects (mean age 21.5 ± 1.65 years). The same data were processed through Nexus (Vicon Motion Systems, Oxford, England) modeling software. The joint angle data was statistically compared between the two systems using a variance components model which determined the variability between maximum, minimum, and range values.

Static accuracy ranged from 99.31% to 99.90%. Static resolution ranged from 0.04 ± 0.15 mm to 0.63 ± 0.15 mm at the 0.05 level of significance. The dynamic accuracy ranged from 94.82% to 99.77 %, and dynamic resolution ranged from 0.09 ± 0.26 mm to 0.61 ± 0.31 mm at the 0.05 level of significance. These values are comparable to those reported for a standard Vicon 524 (Vicon Motion Systems, Oxford, England) motion analysis system. Gait cycle maximum, minimum, and range values showed no significant difference when comparing Visual3D and Nexus at the pelvis, hip, and knee. Significant differences were seen at the tibia (rotation) and foot due to foot model variations between the two systems. The results support application of the lower cost Optitrack cameras and Visual3D software for 3D kinematic assessment of lower extremity motion during gait. Additional potential applications supported by these findings include other lower extremity models, assisted ambulation, and wheelchair mobility.

ACKNOWLEDGEMENTS

Jeffrey D. Kertis, B.S.

There is no feasible way to say that I was able to accomplish this thesis on my own. There are several people that I would like to thank for their help with regards to work that I was able to achieve.

I would first like to thank my father, Robert, and my mother, Karen. Without their support and guidance, I would not be where I am today. They have been there for me in all aspects of my life, both personal and academic. They are the ones who inspired me to pursue an advanced degree and have helped me in every step of the process. I would also like to thank my three brothers, John, James, and Justin, for being a constant support in my life.

My greatest thanks goes to Dr. Gerald Harris who has been my advisor for all of my time as a graduate student. He has shown me the importance of my project as well as the impact it will have on those that are truly less fortunate than myself. Without him, I would have most likely not pursued the field of motion analysis. I am so happy to be part of a project that is improving the lives of so many people.

I would also like to thank the other members of my Committee including Dr. Jason Long, Dr. Peter Smith, and Jessica Fritz. They have guided me and given me invaluable advice and support with my research project and development as an engineer. Without their help, I would not have been able to accomplish many of the goals I wished to achieve during graduate school. I would also like to thank the Orthopaedic Rehabilitation Engineering Center (OREC). All of the staff and fellow graduate students have contributed greatly to my completion of this project.

TABLE OF CONTENTS

LIST OF TABLES

LIST OF FIGURES

I. Introduction

Human motion analysis provides a quantitative means of assessing whole body and segmental motion of subjects with musculoskeletal pathologies. The goal of this work was to assess a low cost motion analysis system appropriate for completing three-dimensional (3D) whole body kinematics. The system has been designed to support lower cost outreach efforts that require accuracy and resolution on the order of classical fixed lot systems. This project addresses the need for reliable data acquisition appropriate for treating children and adults with pathologies who can benefit from a gait analysis assessment.

I.A. Definition of Motion Analysis

Motion analysis covers a wide range of uses. The techniques behind data capture and processing can vary. Some will utilize active markers, others will use passive markers. Some systems will use magnetic fields and others will use infrared cameras to determine the motion of the body. Processing depends greatly on the programming and algorithms used when determining landmarks, i.e. the hip joint center, joint kinematics, and kinetics. However, the end goal remains the same. The general method used for quantitative motion assessment defines a segmental model of the skeletal region of interest with intersegmental joints. This quantitative description of the tri-axial joint motion requires a mathematical model of the system and a series of external markers that are visible to the motion capture system and in proximity to key anatomical landmarks. Each segment is created by a minimum of three markers. A plane is required to represent each segment so that tri-axial rotation can be fully defined. It is typical in the clinical

setting to employ a Cartesian coordinate system embedded into each body segment for calculation of intersegmental joint angles [1].

Optical cameras are used to record the position of the external markers in space as the subject ambulates through a predetermined capture volume. At least two cameras must simultaneously view each marker in order to determine its 3D coordinates. Since each camera can only perceive a two-dimensional (2D) view of the markers, multiple cameras collaborate in determining the 3D location based on the positions of the cameras in space and the location of individual markers in each camera's 2D view. Because some markers can be obstructed from the view of cameras during arm swing and with the use of assistive devices, most systems are redundant with multiple cameras. All cameras are synchronized to record marker position at the same time using a frame rate between 50 and 250 frames per second [23 – 26].

There are a variety of marker sets currently used to accurately determine joint kinematics. The marker set used for this study is a modified Helen-Hayes model. In the original Helen-Hayes model, two markers are placed on the right and left anterior superior iliac spine (ASIS). Another marker is placed between the two posterior superior iliac spines (PSIS) and labeled as the sacral marker. Four more markers are placed on either side of the lower extremities which include the greater trochanter, lateral femoral epicondyle, lateral malleolus, and space between the second and third metatarsal heads. Two more markers are positioned on either side, with the use of marker wands roughly 7 cm longs, at mid-thigh and mid-shank. Regression equations and other algorithms can be used to determine the hip joint center based off of anthropomorphic data. The knee center is assumed to be halfway between the medial and lateral femoral epicondyles, in a plane

with the thigh-wand marker, and the hip joint center. The ankle joint center is assumed to be halfway between the malleoli in a plane defined by the ankle marker, knee center, and shank-wand marker [7]. In the modified Helen-Hayes model, the greater trochanter markers have been removed, and markers have been added to the heel of each foot. This allows for a better representation of the foot segment [30]. Figure 1 helps better describe the positioning of the markers used in the modified Helen-Hayes model.

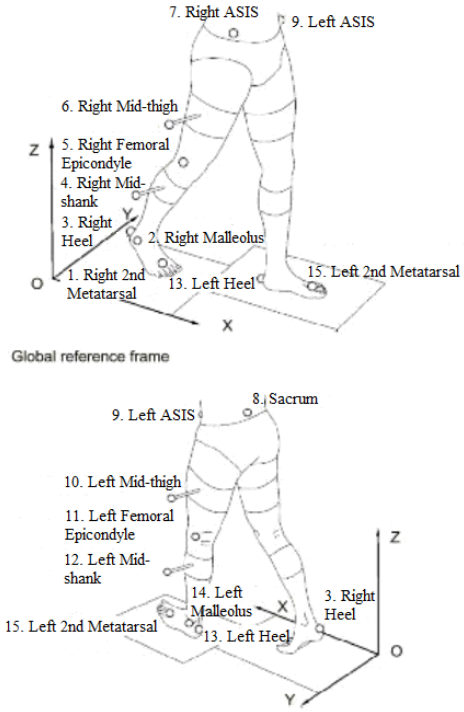

Figure 1: Modified Helen-Hayes Marker Set [35].

Once the marker positions have been located in 3D space, associated labels are applied to each marker to define anatomic location, i.e. RASIS: Right Anterior Superior Iliac Spine. Biomechanical modeling software is then used to determine joint orientation and motion between segments [1].

In gait analysis, determining joint kinematics is the first step in performing a complete assessment. The angles of rotation for the pelvic coordinate system are typically taken with respect to the global coordinate system or with respect to a trunk coordinate system. The hip joint angles are determined by the thigh local coordinate system rotation with respect to the pelvis local coordinate system. The knee joint angles are determined by the rotation of the shank coordinate system with respect to the thigh coordinate system. Finally, the ankle joint angles are determined by the rotation of the foot coordinate system with respect to the shank coordinate system. In place of looking at the joint rotation in the coronal plane of the foot with respect to the shank, the ankle is assessed by comparing the rotation of the foot with respect to the global coordinate frame in the transverse plane which is typical of most gait reports. This is known as the foot progression angle. Euler angles are applied to describe the relative rotation of one segment with respect to another in 3D space. These angles are described by three finite rotations in succession to achieve the final orientation from the reference orientation, i.e. the more proximal body segment. When calculating Euler angles, it is necessary to define a set of orthogonal embedded axes for the dynamic and reference segments. Typically, the X-axis is along the walkway, the Z-axis is vertical pointing upward, and the Y-axis is perpendicular to both X- and Z-axes, which forms a right-hand Cartesian coordinate system. When a particular segment rotates an angle α about the reference Y-axis, the resulting angles with reference to a lower extremity model are pelvic anterior or posterior tilt, hip flexion or extension, knee flexion or extension, and foot dorsi or plantar flexion. Now the new orientation of the local coordinate system of the moving segments is denoted as X_1, Y_1, and Z_1. When the segment rotates an angle β about the X_1 axis, the

rotations are defined as pelvic obliquity, hip abduction or adduction, and knee varus or valgus. The ankle is separately considered as described earlier. The new orientation of the moving segment axes are denoted as X_2, Y_2, and Z_2. With the final rotation of angle γ about the new Z_2 axis, the rotations are defined as internal or external pelvic, hip, tibial, and foot rotation. The rotation matrix associated with this calculation is shown in equation 1:

$$R = \begin{bmatrix} \cos\alpha\cos\gamma + \sin\beta\sin\alpha\sin\gamma & \cos\beta + \sin\gamma & -\sin\alpha\cos\gamma + sin\beta\cos\alpha\sin\gamma \\ -\cos\alpha\sin\gamma + \sin\beta\sin\alpha\, cos\gamma & \cos\beta\cos\gamma & \sin\alpha\sin\gamma + \sin\beta\cos\alpha\cos\gamma \\ \cos\beta\sin\alpha & -\sin\beta & \cos\beta\cos\alpha \end{bmatrix} \quad (1)$$

This Euler rotation gives the change in angle of all four joints in all three planes of motion. There are other orders of rotation done in calculating Euler angles, but this is the most common one used in the clinical field [7]. Figure 2 represents the Euler rotations.

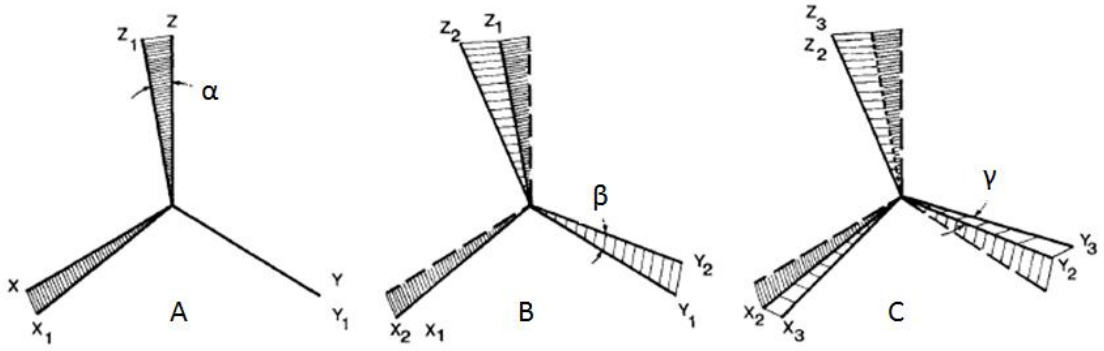

Figure 2: Euler Rotation [7]

During kinematic assessment, many temporal parameters can also be determined. The most common parameters taken into consideration are cadence, walking speed, step length, and stride length. Cadence is the number of steps taken per minute. Walking

speed is the number of meters walked per second. Step length is the distance between the heel strike of one foot to the heel strike of the opposite foot, and stride length is the distance between the heel strike of one foot to the consecutive heel strike of the same foot. Typically, force plates and EMG electrodes are simultaneously used in calculating joint kinetics and muscle activity. This helps in determining moments and power at the joints as well as determining if muscles have appropriate firing patterns. With all of this information, the gait characteristics of a person can be extensively described.

I.B. Current Applications and Clinical Needs

Motion analysis systems have been used in the clinical setting for pre-treatment and post-treatment follow up of persons with upper and lower extremity pathologies. The biomechanical effects of Lofstrand crutches were evaluated using an upper extremity model to help patients with myelomeningocele (MM) [2]. This model utilizes a marker set that separates the upper body and crutch into four bilateral segments including the upper arm, forearm, hand, crutch, and thorax. Both kinematics and kinetics were used to examine motion patterns in these children as compared to a control population. Evaluation showed significant differences between reciprocal and swing-through gait patterns with respect to joint angle ranges. The authors reported that the model offered a valuable tool for assessment of children with MM, which was appropriate for further applications. Reliability and repeatability of upper limb kinematics is also important when modeling children with cerebral palsy (CP). Models have been assessed for both of these factors and have shown that marker sets used to determine joint kinematics provide high inter and intra subject repeatability and reliability [42, 44]. Full motion analysis and energy expenditure has been compared during walker-assisted gait for children and adults

with CP in order to assess treatment options [3, 4]. Arm splints have also been evaluated in improving movement fluency in children with CP in which a significant difference was seen in terms of movement substructures after three months of Lycra® arm splints [43]. In addition, motion analysis has been used to compare the affected and unaffected arms of post-stroke persons. The authors reported that the upper extremity kinematics aided rehabilitation planning and were effective in reducing recovery times [5]. Even more precise kinematics can be evaluated using finger segment models. These models allow the assessment of movements for more workplace tasks such as typing, small part assembly, and powered hand tool operation. This information can look at improvements of range of motion for those with disabilities affecting fine motor control [45].

Determining upper extremity kinematics of subjects in wheelchairs also utilizes similar biomechanical models. Often times, the biomechanics of different propulsion patterns are assessed to increase performance while reducing internal joint forces, particularly the glenohumeral and radiocarpal joint. Parameters such as cycle frequency, push time, recovery time, and push angle can be determined for wheelchair users. Typical wheelchair users who can benefit from upper extremity motion analysis assessment include those with spinal cord injury, MM, neuro-muscular pathologies and similar motion-restrictive conditions [2, 6].

Lower extremity models are most frequently applied in assessment of gait pathologies. These models can be used for general lower extremity analysis as well as more detailed segmental analysis of the distal extremities. Normal control kinematics are frequently used to compare pathologic gait patterns [7, 8]. Ensuring that gait patterns can be determined for control subjects is vital in its use for comparative purposes with

subjects who have gait abnormalities. Different models have to be assessed against one another in order to determine the simplest and most effective model to be used [51]. CP is one of the more commonly analyzed pathologies that utilize lower extremity motion analysis for selection of treatment options [9, 10]. Areas of investigation with regards to gait in children with CP include helping to distinguish differences between CP and hereditary spastic paraplegia (HSP) and more in depth investigations regarding coronal plane alterations for children with hemiplegic CP [52, 53].

Osteogenesis imperfecta (OI) is a pathology that has received more recent attention in utilizing the benefits of lower extremity gait analysis. A comparison between control subjects and those with OI showed that the OI group demonstrated increased double limb support, delayed foot off, and decreased ankle range of motion and plantar flexion during the third rocker [22]. Assessing push-off power during gait is a more focused aspect of OI when looking at the ankle. The study found that due to weaker plantar flexors, the children had a reduced ankle power production and sagittal plane ankle angular velocity [36]. The authors noted that results could be used to gain a better understanding of OI and to help improve treatment planning and overall quality of life. Kinetics have also been incorporated into assessments of subjects with OI. Quantified loading conditions at the femoral head, diaphysis, and condyles are one area of assessment. The authors implemented these into a finite element model to determine the risk of femoral fracture during gait for a person with OI type I. The modeled OI femur showed no risk of fracture during gait and that the highest stress level occurred during mid-stance and loading response phases of gait [13].

In addition, motion analysis can be used to influence decision making for orthopaedic surgery and assess post treatment progress [54, 55]. Other areas of lower extremity motion analysis applications include resistance training for multiple sclerosis (MS), cast techniques for children with clubfoot, knee kinematics in Blount's disease, effects of obesity on stair walking, and knee buckling in subjects with inclusion body myositis [11, 12, 14, 56, 57].

More detailed segmental motion models have been recently reported for assessment of foot and ankle pathologies. Rankine et al. used the number of segments to classify different foot models. Typical models of the foot include the hindfoot, midfoot, forefoot, and great toe (hallux). Popular foot and ankle models include the Milwaukee foot model (MFM) which uses an x-ray reference for marker placement, the Oxford model which uses a tibial alignment jig, and the five-segment model of Leardini [15]. Foot pathologies affecting the hallux, such as hallux valgus and hallux rigidus, along with posterior tibial tendon dysfunction (PTTD) have been assessed with the MFM to better identify treatment options and to compare post-operative outcomes [16–19]. Other models have been used to evaluate general walking on level ground and treadmills, rheumatoid arthritis, the effects of subtalar kinematics on the dynamic function of the tibialis anterior, soleus, and gastrocnemius muscles, and post-operative evaluations of subjects with ankle fractures [47–50]. Foot and ankle models can also be applied to evaluate the effects of inserts, orthotics, or shoe modifications. Rocker sole shoes for relief of high plantar pressure loads occurring with diabetic neuropathy have also been studied [20, 21]. Motion analysis has also been used to evaluate the capability of stiffness-adjustable ankle-foot orthotics (AFO) and its affect on ankle joint kinematics.

They were shown to reduce both dorsi and plantar flexion [46]. This is just a sample of the potential applications for motion analysis and the benefits clinicians and physicians can obtain from the data it provides.

I.C. Current Systems Available

There are a wide variety of motion analysis systems currently available on the market today. The most prevalent systems will be discussed here. Vicon (Vicon Motion Systems, Oxford, England) is one of the most traditional systems currently being used in the clinical setting. The system offers standard components typically used by researchers or clinicians during gait analysis. The system utilizes Nexus software to record movement data along with synchronized signals from other measurement devices including EMG (electromyography) and force plates. Vicon Nexus offers several features to automate processing including automatic marker labeling and event detection (i.e. foot strike and foot off). Vicon's Polygon software allows post processing to display joint kinematic and kinetic data as well as EMG patterns [23]. Figure 2A represents the cameras used by Vicon for collecting marker data.

Another motion analysis system is the Optotrak Certus (Northern Digital Inc., Ontario, Canada). Optotrak incorporates a "Smart Marker" system of active markers. Battery powered strobes eliminate the need for wires. Up to 50 strobes can be used at a time per battery system. The Optotrak software allows for incorporation of force plates, EMG, eye-trackers, and other third party instrumentation. The Optotrak motion analysis system is compatible with other software including Visual3D which is used for higher level data processing by multiple vendors [24].

Motion Analysis Corporation (MAC) (Santa Rosa, CA) is another company that provides motion analysis systems for gait analysis. Much like the Vicon system, MAC uses passive markers. The main motion capture software called Cortex is used for all phases of recording including calibration, tracking, and post processing. These systems also allow simultaneous analog data input from force plate and EMG sources. Cortex is used to calculate and display kinematic, kinetic, and EMG data. SIMM (MusculoGraphics, Inc., Santa Rosa, CA) is software supplied by MAC which is used for monitoring changes in muscle length and muscle moment arms during gait [25]. This software can also be used with any gait analysis software including Vicon.

Systems can also be developed by combining hardware, data capture, and processing software. A recent development described here is a combination of Optitrack Cameras (NaturalPoint, Inc., Corvallis, OR) and Visual3D and AMASS (C-Motion Inc., Germantown, MD) software. This is a fairly new combination with little research on the system performance. The hardware includes V100:R2 motion capture cameras which are much smaller than the standard Vicon or MAC cameras. The V100:R2 cameras measure 45.2 mm x 74.7 mm x 36.6 mm with a weight 0.1 kg (Figure 2B). The AMASS software is used for capturing and labeling marker data while Visual3D software is used for kinematic analysis and external signal synchrony (EMG, force plate) [26].

Figure 3: 2A) Standard Vicon motion capture camera [64]. 2B) Standard Optitrack motion capture camera [65].

The Optitrack motion capture cameras have previously been used in the area of gait. A study by Leo et al. proposed to create a novel interactive mobile floor projection game system for pediatric gait and balance training. The system projected a virtual environment on the floor of a room and the Optitrack cameras would pick up the person's motion. The system is targeted to retain attention for children and increase motivation [39, 40]. Another example of the Optitrack cameras being used in human gait is a study by Watanabe et al. where a camera is worn on the leg in an attempt to determine the walking pattern of the subject from the images recorded by the camera [41]. Simultaneously, Optitrack cameras are used to capture motion data of the subject to compare data calculated from the camera worn at mid-thigh on the subject in the attempt to find algorithms that can correlate walking patterns in an outdoor environment without the need of a motion analysis system.

I.D. Significance of Current Study

Two independent factors to consider when developing a system are cost and performance. Listed below is a comparison of performance characteristics of all systems described herein (Table 1). The first three systems have been tested for accuracy, precision, and/or resolution [27–29]. Traditionally, motion analysis system prices can range from $50,000 – $300,000, which may not be affordable for some clinics and hospitals, particularly those in underdeveloped countries. The combination of Optitrack cameras and C-motion software may provide a less expensive alternative with the hardware and software priced at less than $50,000. The static and dynamic calibration of the cameras and kinematic data comparison from this combination of motion analysis hardware and software will be discussed further with respect to its potential use for a less expensive, yet reliable, motion analysis system. If successful, this combination system will provide a broader population to undergo gait analysis and whose ability to ambulate could be greatly improved from the information surgeons and physicians obtain from these assessments.

Table 1: Motion Analysis system performance parameters.

	Markers	Sampling Rate (frames/sec)	System Resolution(mm)	Precision (mm)	System Accuracy (%)
Optitrack	Passive	50-100	0.63	-	94.82
Vicon	Passive	120-250	1.49	-	98.30
Optotrak	Active	50	-	0.03	98.44
Cortex (MAC)	Passive	200	-	-	-

II. Methods

II.A. Instrumentation for System Characterization

An eight-camera Optitrack V100:R2 (NaturalPoint Inc., Corvallis, OR) motion capture system was used to acquire 3D marker data at 100 frames per second (fps) with 15.9 mm diameter markers. The cameras utilize a 4.5 mm lens with a horizontal field of view (FOV) measuring 46 degrees. The image parameters include a pixel size of 6 µm x 6 µm and an image resolution of 640 x 480. ARENA motion capture software (NaturalPoint Inc., Corvallis, OR) was used to acquire the 3-D marker data. A reference cone was used for static testing while a combination of the cone and a bar were used for dynamic testing represented by figures 4A and 5A, respectively. The combination consisted of a Styrofoam™ cone cut in half and a Styrofoam™ bar, each having reflective markers placed at predetermined distances.

For angular dynamic testing, a Biodex System III (Biodex Medical Systems, Shirley, NY) was employed to generate a defined angular velocity. The Biodex was used for angular dynamic testing since the system can be set to rotate in a plane of choosing at pre-set angular velocities [27].

II.B. Static and Dynamic System Characterization

Resolution and accuracy for the Optitrack motion capture system were determined statically and dynamically [27, 28, 30, 31]. For static linear testing, three markers were placed on the reference cone at predetermined distances associated with typical foot marker distances [27, 28] (Figure 4A). The short foot and long foot distances measured 57.5 mm and 140.6 mm, respectively. The short foot distance was selected as a

representative foot distances measured from the heel to the ankle and the long foot distance was from the ankle to the toe. The reference cone was placed along the Cartesian coordinate axes and positioned to face the center of the capture volume (Figure 4B). The locations consisted of opposite corners of the gait walkway measuring 1.1 m x 3.1 m, opposite edges of the twin force plates in the center of the walkway, and the center locus between the force plates. A 3-second trial was recorded at each of the five locations. Marker data was processed by performing marker labeling in ARENA and exported for statistical analysis in MATLAB. Since ARENA requires labeling rigid bodies to export C3D file data, a c3dserver package was installed and MATLAB code was written (Appendix A) to combine multiple C3D files into one for easier processing. For linear dynamic testing, the cone and thigh/leg bar were fixed to each other to represent a leg with typical marker placement (Figure 5A). Five markers were located on the thigh/leg bar at 205.3 mm, 417.8 mm, 181.6 mm, and 397.2 mm, representing the approximate distances for hip to mid-thigh, hip to knee, knee to mid-calf, and knee to ankle, respectively. These marker locations are analogous to those used for whole body lower extremity and upper extremity (walker, crutch, cane, and wheelchair) analyses [10]. Marker distances used for the reference cone were identical to those of the static testing. The entire lower extremity system (cone and thigh/leg bar) was then translated five times each way at a free walking speed through the capture volume in the positive and negative X-direction.

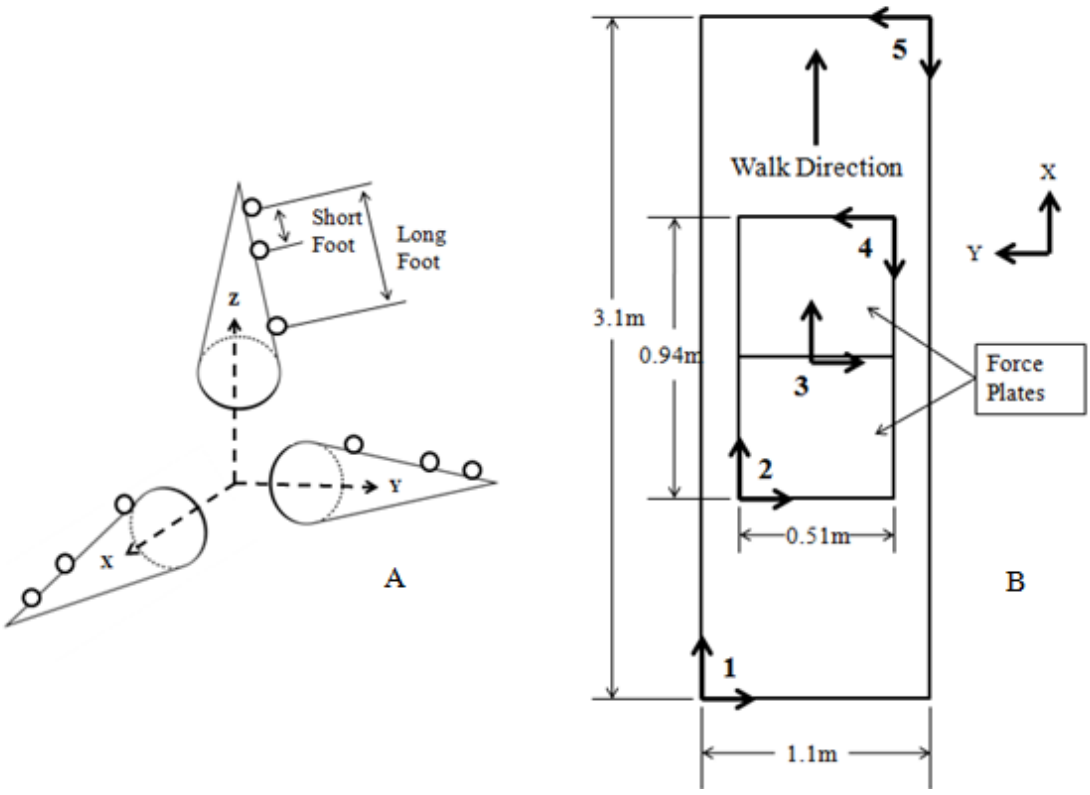

Figure 4: A) Static testing Tri-Axial Calibration Cone. B) Calibration space with locus for static testing.

Angular dynamic testing employed the Biodex System III to rotate through a range of 305 degrees. Five markers were placed on a Biodex attachment arm at distances of 57.5 mm, 140.6 mm, 205.3 mm, and 417.8 mm from the origin of rotation (Figure 5B). The marker distances describe those used in typical gait analysis and are analogous to those of the linear dynamic testing. The Biodex was programmed to rotate through a range of 305 degrees at 90 deg/sec. Data were recorded for five trials in all three planes of motion (XY, XZ, YZ) during clockwise and counterclockwise rotation. A 2 second portion, in which the angular velocity was calculated to be constant, was used for analysis.

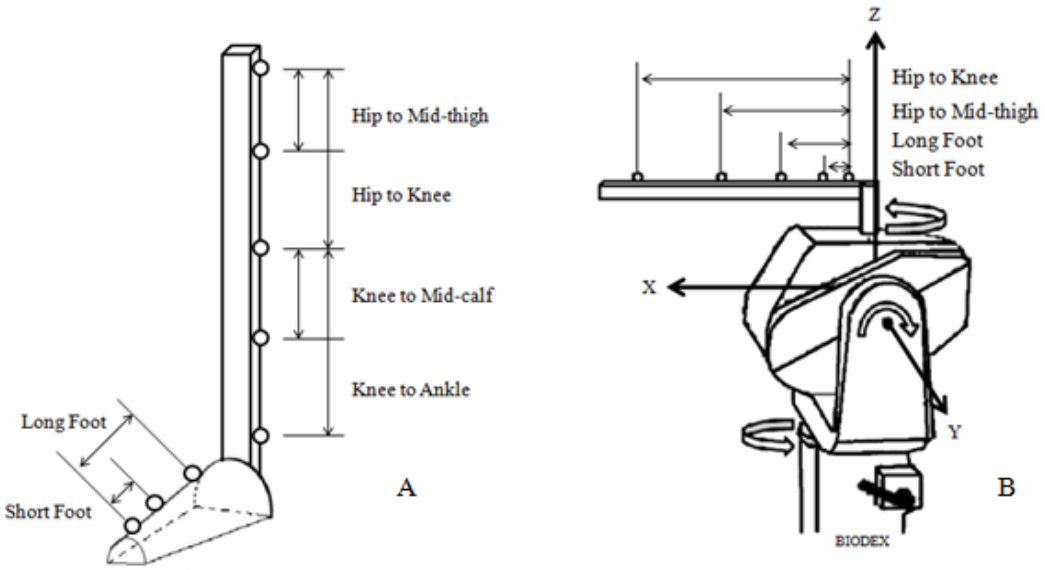

Figure 5: A) Linear dynamic calibration frame. B) Biodex with rotational dynamic calibration frame. Marker distances are representative of those used in human gait.

In order to assess the reliability of the Optitrack cameras, system resolution and accuracy equations were applied to the data collected. System resolution was calculated using the following equation [27, 28]:

$$R = \left| D - \frac{1}{n}\sum_{i=0}^{n-1} d_i \right| \pm t\left(\frac{s}{\sqrt{n}} + \varepsilon_r + \varepsilon_m\right) \quad (2)$$

Where R is the system resolution; D is the measured (empirical) distance; n, total number of samples; d_i, computed distance; t, t-test coefficient [27]; s, sample standard deviation; ε_r, round-off error = $(5/10^m)$; ε_m, measurement error based on micrometer resolution (±0.02mm); and m, number of significant digits. A p-value of 0.05 and 0.01 was used for analysis.

System accuracy was computed as [27, 28]:

$$A = \left(1 - \frac{\left| x_w - \frac{1}{n} \sum_{i=0}^{n-1} d_i \right|}{\frac{1}{n} \sum_{i=0}^{n-1} d_i} \right) \times 100\% \quad (3)$$

Where A is the system accuracy as a percentage and xw is the worst data point. The average value of the computed distance was used as an estimate of the true distance between markers because of measurement error [33].

II.C. Subject Population

The participants in the study were 10 control subjects (5M and 5F) between the ages of 19 and 24 (mean age 21.5 ± 1.65 years). The height of the subjects was between 1.80 and 1.57 meters (male mean height: 1.78 m ± 0.04 m, female mean height 1.64 ± 0.05 m) and the mass was between 58.97 and 79.37 kg (male mean mass 73.29 kg ± 3.74 kg, female mean mass 60.06 kg ± 4.26 kg). Participants in the study were required to be between the ages of 18 and 30 and have no orthopaedic or neuromuscular impairment that affects lower extremity motion. Table 2 represents subject characteristics. Subject D was excluded because after data collection, it was found that the pelvic (left and right ASIS and sacral) markers had too much drop out due to the subject's height. Each subject wore shorts and a t-shirt. The shorts were required to be rolled up so that the mid-thigh marker was visible to the cameras. The t-shirt was also rolled up so that the markers on the pelvis were visible. In addition, the subjects walked barefoot so that markers could be placed properly on the heel, lateral malleoli, and second metatarsal.

Table 2: Subject characteristics.

Subject	Gender	Age	Height (m)	Weight (kg)
A	Male	23	1.8034	72.57
B	Female	19	1.7272	54.43
C	Female	23	1.6256	58.967
E	Female	22	1.5748	58.967
F	Female	21	1.6002	60.327
G	Male	22	1.8034	71.667
H	Female	19	1.6764	67.585
I	Male	24	1.8034	79.37
J	Male	21	1.7018	68.04
K	Male	21	1.778	74.84

II.D. Subject Testing with Optitrack/Visual3D

The cameras were positioned on four tripods with two cameras on each tripod. The four tripods were placed in a room to create a rectangle measuring 10 m x 20 m. Two additional cameras were placed at either end of the capture volume along the path that the subjects would walk. Camera positions were adjusted so that calibrating the L-frame, which represents the origin (0, 0, 0), would be in the center of each camera's field of view during calibration. The capture volume was then calibrated in order to collect marker data. AMASS (C-Motion, Inc. Germantown, MD) was used to calibrate the capture volume as well as subject data. Settings within AMASS were set to include "units" as mm, "predictor error" as 3mm, "minimum cameras" as 2, "maximum residual" as 0.5mm, and "connect gap" as 10 frames. The first file recorded was the calibration file. A calibration wand with predetermined marker distances was waved for a total of 50 seconds within the capture volume to determine the 3D position of the cameras with respect to the origin. During the calibration process, the cameras are linearized to account for the curvature of the camera lens. Once this was completed, the calibration file was

processed to ensure that every camera was detected and error values were within tolerance limits. Images of the capture volume as well the L-frame and wand can be seen in Appendix D.

Fifteen reflective markers (d = 14mm) along with knee alignment devices (KADs) were placed on each test subject. The marker positions represent those seen in figure 1. The following labels were given to the markers used for both static and dynamic trials: LASI (Left Anterior Superior Iliac Spine), RASI (Right Anterior Superior Iliac Spine), SACR (Sacrum), LTHI (Left Mid-Thigh), RTHI (Right Mid-Thigh), LKAX (Left KAD Axial), LKD1 (Left KAD Upper), LKD2 (Left KAD Lower), LKNE (Left Knee), RKAX (Right KAD Axial), RKD1 (Right KAD Upper), RKD2 (Right KAD Lower), RKNE (Right Knee), LTIB (Left Shank), RTIB (Right Shank), LANK (Left Lateral Malleoli), RANK (Right Lateral Malleoli), LHEE (Left Heel), RHEE (Right Heel), LTOE (Left Second Metatarsal), and RTOE (Right Second Metatarsal). The KADs (Knee alignment device) were used during static trials to independently define the axis for knee flexion/extension prior to the dynamic trials. The use of KADs during the static trial eliminates the need for a medial knee marker which can be knocked off during ambulation. The KAD is a spring loaded metal jig that fits gently over the subject's knee such that the supports are in contact with the medial and lateral femoral epicondyles. The orientation of the KAD allows software to calculate the relative transverse alignment of the axis to the transverse plane orientation of the thigh and shank. The correct alignment of the thigh and shank wands becomes less critical as any minor alignment errors can automatically be removed during processing of the dynamic trials. Figure 6 shows a KAD used during gait analysis.

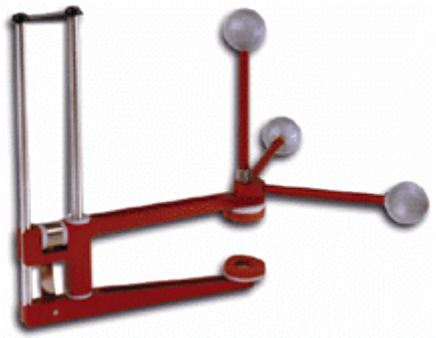

Figure 6: Knee alignment device (KAD) used to determine the knee flexion/extension axis [66].

Markers were placed such that the pelvis, thighs, shanks, and feet were represented by a plane made up of three markers. The marker set used is the modified Helen-Hayes model discussed in section I. A. Before markers were placed, a series of anthropomorphic measurements were taken, including, height, weight, inter-ASIS distances, ASIS to lateral malleolus, ASIS to medial malleolus, thigh radius, knee width, ankle width, and bilateral anteriorposterior (AP) distance (ASIS to greater trochanter) which is used to help calculate the hip joint center. Equation 4 was used to determine the AP distance [68].

$$AP\ (meters) = 0.1288 * (Average\ Leg\ Length) - 0.04856 \quad (4)$$

These parameters were used when applying the biomechanical model to the marker data for both Visual3D (C-Motion, Inc. Germantown, MD) and Nexus (Vicon Motion Systems, Oxford, England). ASIS to lateral malleolus was used for Visual3D and ASIS to medial malleolus was used for Nexus.

The subject stood in the center of the capture volume while wearing the 13 markers with the KADs, where two additional markers will replace the KADs for a total

of 15 after the static trial. A five second static trial was recorded that was used to apply the biomechanical model. Three static trials were recorded to ensure that at least one trial will have minimal marker dropout and be able to be used to attach the biomechanical model. The KADs were then replaced with two reflective markers placed on each lateral femoral epicondyle (LKNE and RKNE). The subject then stood at the end of the capture volume and proceeded to ambulate at a self-selected walking pace to the other side of the room (a distance measuring approximately 5 meters in the positive y-direction). AMASS was used for data recorded at a rate of 100 fps. Ten second trials were used to ensure sufficient time for the subject to start and end within the designated time frame. Twelve trials were recorded with the subject starting on the left foot for the first six and the right foot for the second six. Six trials were collected for each side since symmetry was not assumed. An average of seven steps was able to be completed during each trial with the subject starting from the same side of the capture volume. The cameras were positioned to record the marker data of the middle three to four steps to allow for normal gait to be achieved and sufficient space to stop and for a consistent gait pattern before the end of the walkway. From each side, three trials were selected with the least amount of marker dropout for marker labeling and use in the Visual3D software for kinematic analysis. For each trial, the markers were labeled according to appropriate anatomical landmarks as previously listed.

The model that was applied to each static trial was created in Visual3D. Within the “Models” portion of the software, segments and joint centers can be created using the static trial. First the pelvis was created by selecting the LASI, RASI, and SACR markers. The left and right KAD segments were then created, which were selected only for

kinematic use. The RKAX, RKD1, and RKD2 markers were selected to create the knee joint center. This process was also repeated for the left side. The right thigh was then created. This included defining the proximal joint as the HH_RIGHT_HIP (Helen-Hayes right hip) landmark, which was defined when the pelvic segment was created, and the distal joint as the HH_RIGHT_KNEE_FROM_KAD (Helen-Hayes right knee joint center based off the KAD) landmark. Radii were also applied with the proximal joint using the thigh radius and the distal segment radius as:

$$r = 0.5 * Right\_Knee\_Width + Marker\_Radius \quad (5)$$

An extra target was defined as the RKNE marker that replaced the KAD. Tracking targets were then selected as HH_RIGHT_HIP, RKNE, _HH_RIGHT_KNEE_FROM_KAD, and RTHI. This same process was repeated for the left thigh. The right shank segment was then created. The HH_RIGHT_KNEE_FROM_KAD landmark was selected as the proximal joint and the radius was describes as:

$$r = 0.5 * Right\_Knee\_Width + Marker\_Radius \quad (6)$$

The RANK marker was selected as the lateral joint used for the distal portion of the segment with a radius of 0.5*Right_Ankle_Width+Marker_Radius. RTIB was used laterally as an extra target to define the orientation. Tracking targets were then selected as RKNE, HH_RIGHT_KNEE_FROM_KAD, RTIB, and RANK. This was repeated for the left shank. This is assuming that the axis or rotation is going directly through the knee marker. The right foot was then created. The proximal joint was defined laterally by the RANK marker and the joint was defined as the HH_RIGHT_ANKLE (Helen-Hayes right ankle) landmark that was created based off marker positioning. The distal joint was

defined as the RTOE marker. The radius for the distal marker was arbitrary, so it was set at 0.06 m. The tracking target markers used for the foot included HH_RIGHT_ANKLE, RANK, RHEE, and RTOE. This was repeated for the left foot. Two additional landmarks labeled R_HEEL_Z and L_HEEL_Z were created with an offset of -0.1 in the vertical direction with respect to the heel markers. This will be used to create a coordinate system to better calculate the ankle joint angles. The right side segment was labeled "Right Virtual Foot" and was labeled as kinematic only. RHEE was defined as the proximal joint and RTOE was defined as the distal joint. The radii were arbitrary and a value of 0.01 m was selected. The extra target used to define the orientation was the R_HEEL_Z landmark. The tracking target markers were the HH_RIGHT_ANKLE, RHEE, and RTOE. The segment coordinate system was centered at the heel marker with the y-axis as anterior/posterior, the x-axis as medial/lateral, and the z-axis as vertical. This will ensure that the y-axis is parallel to the floor and the z-axis is vertical. This process was repeated for the left side. Once all of the segments had been created, subject data parameters were altered to be associated with the subject. Mass, height, HH_Asis_Distance, HH_AP_Distance (anterior posterior distance), HH_Right_Leg_Length, HH_Left_Leg_Length, Right_Knee_Width, Left_Knee_Width, Right_Ankle_Width, and Left_Ankle_Width were altered in the Subject Data/Metrics portion of Visual3D.

Once the model was applied to each subject, the dynamic trials were implemented into Visual3D for processing. Each of the 10 subjects contributed three trials to both the right and left side for analysis. Three separate trials for both left and right sides were used because the capture volume was limited, and some of the trials were unable to record a

full stride for both left and right side of the body depending on the person's stride length. All of the dynamic trials were selected and joint angles were created for the model. Table 3 shows the name of each joint angle created as well as which axes were negated, i.e. flipped over the x-axis when plotting, which segment is moving and with what segment it is in reference to. For each joint, the normalization was off and the Cardan sequence was X-Y-Z.

Table 3: Name, axis negated, segment, and reference segment used to calculate joint angles.

Data Name	Negate	Segment	Reference Segment
Left Ankle	Z	Left Virtual Foot	Left Shank
Left Foot Progression	Z	Left Virtual Foot	LAB
Left Hip	Y,Z	Left Thigh	Pelvis
Left Knee	X,Y,Z	Left Shank	Left Thigh
Left Pelvis	X,Z	Pelvis	Lab
Right Ankle		Right Virtual Foot	Right Shank
Right Foot Progression		Right Virtual Foot	LAB
Right Hip		Right Thigh	Pelvis
Right Knee	X	Right Shank	Right Thigh
Right Pelvis	X,Y	Pelvis	LAB

Each walking (dynamic) trial was opened within the "Signals and Events" tab of Visual3D. Heel strike was determined by looking at the heel marker and selecting the frame at which there is no more forward movement of the maker. Toe off was determined by selecting the frame at which there was significant forward motion of the metatarsal marker trying to ignore any movement due to noise.

A report was created in which the joint angles were plotted for the left and right side of the body for the pelvis, hip, knee, and ankle in all three planes of motion. Foot progression replaced the coronal plane portion for the ankle. Once the results were plotted, the data was interpolated with a maximum gap of 10 frames using a 3rd order

polynomial. The data was also run through a Butterworth filter with a cut off frequency of 6 Hz. The joint angle data for the 60 trials were exported into a spreadsheet which was used for the statistical analysis. Temporal parameters, including speed, stride length, step length, and steps per minute were also calculated based on foot strike and foot off information.

The marker position data recorded from AMASS was also processed using Vicon's Nexus software. The static marker file was opened and labeled the same as in Visual3D. The "KAD PlugInGait (SACR) model was attached to the static file and the anthropomorphic data was inserted. In the pipeline, "Static Plug-in Gait (KAD)" was run which runs a VPI Compatibility static gait model. The "PlugInGait (SACR) model was then attached, which replaces the KADs with a single knee marker on the femoral epicondyle. Under the pipeline, "Static Plug-in Gait" was selected and run. This is done to calibrate the Plug-in Gait model for each subject. Each dynamic trial associated with each subject's static trial was opened and labeled.

In addition, foot strike and foot off were determined for each trial by going through each file and selecting the frame that the heel markers stops moving forward for foot strike and the second metatarsal marker starts moving for foot off. The ability to track the path of each marker individually made this process easier. In Nexus, foot strike is the same as heel strike in Visual3D and foot off is the same as toe off in Visual3D.

Gaps were also filled by highlighting the marker name that is missing and selecting "pick source" and "fill" under the "pattern fill" option. A marker affiliated with the missing marker, usually part of the same segment (i.e. RASI if LASI has a gap), is used for the source. Under the pipeline, "Dynamic Plug-in Gait Labeled" was run, which

deletes unlabeled trajectories, applies a Woltring filtering with a default mean squared error of 10, VPI Compatibility Run dynamic gait model, and exports a C3D file. The pipeline was changed to "Export" to generate gait cycle parameters and create an ASCII file where joint angle data and temporal parameters can be selected.

Since each exported file contained joint angle data for both sides and values outside of the desired range, a MATLAB file was created in which only the desired sections were taken (Appendix B). For each trial, slight alterations were needed according to the frame window and the file used to gather the data. In addition, it was required that the data be based off of percent gait cycle. Another MATLAB file was created to convert each data into a percent gait cycle column of data (Appendix C).

For the Plug-in Gait model, the foot is created in the static trial by using the ankle joint as the center with the primary axis toward the metatarsal marker but parallel to a line created by the heel and metatarsal marker labeled as the z-axis in Nexus. The y-axis is defined perpendicular to this based off any tibial rotation and is directed laterally using the ankle marker as reference. The x-axis is then orthogonal to both of these axes and is directed down. This is the main discrepancy seen between the Nexus Plug-in Gait model and that created in Visual3D.

II.E. Comparative Normal Sample

The joint angles determined in this study from Visual3D were qualitatively compared to a study performed by Graf et al. This study was designed to look at the long-term outcomes in young adults following clubfoot surgical release. In the study, gait, strength, segmental foot motion, and outcome questionnaire data was collected on 24 adults (21.8 ± 2.3 years) who were surgically treated for congenital talipes equinovarus

(CTEV) as infants. This data was compared statistically with 48 age group matched controls. The control group contained 29 males and 19 females (23.3 ± 2.4 years). The joint angle data was collected in the Medical College of Wisconsin Department of Orthopaedic Surgery's Motion Analysis Laboratory at Froedtert Memorial Lutheran Hospital. Quantitative gait analysis was performed using a 15-PULNiX camera 3D motion analysis system (Motion Analysis Inc., Eugene, OR) and two force-plates (AMTI, Newton, MA) embedded in the walkway. Joint angle data was processed using Vicon Workstation 5.2.4 software and the Plug-In-Gait model which uses the modified Helen-Hayes marker set previously described in section I.A. This is the same model that is used in the current Vicon Nexus software. In addition, the Milwaukee foot model (MFM) was used to measure the motion of the different foot segments [37]. The ankle joint data was only used for statistical analysis in the study. For the purposes of comparison with Visual3D, the joint angle data for all of the joints were obtained.

II.F. Statistical Analysis

For statistical analysis, a variance components model was applied to the data [58, 59]. This model assumed that there were four independent sources of variability involved in the measurements (subject, side of the body (foot), system, and all others aggregated in the error term). Thus, the total variance was divided into four components and the likelihood ratio tests explored their significance. The main interest was if a system change (Nexus vs. Visual3D) showed a significant contribution to the total variability of the measurements. Percent contribution to the total variance, a generalization to the intraclass correlation coefficient, was used to describe the effect of system change on a parameter of interest. The variance components models mathematically represented as:

$$Y_{ijkl} = \beta_0 + P_i + F_{j(i)} + S_k + \varepsilon_{ijkl} \quad (7)$$

where Y_{ijkl} is a measurement of a parameter of interest with the index i enumerating subjects $i = 1, \dots, 10$), j denotes the side of the body (foot) index (1=Right, 2=Left), k denotes system (1 = Visual 3D, 2 = Nexus), and l enumerates trials ($l = 1, \dots, 3$). β_0 is the average value for the entire population. The model has four random effects: person random effect $P_i \sim N(0, \sigma_P^2)$, the (nested) random effect of the side of the body $F_{j(i)} \sim N(0, \sigma_F^2)$, the random effect of the system $S_k \sim N(0, \sigma_S^2)$ and all other sources of variability including measurement error are absorbed by $\varepsilon_{ijkl} \sim N(0, \sigma^2)$.

The above analysis of the system effect based on variance components was complemented by the person-level analysis. Since subjects represent independent experimental units in the study, an average of all measurements made for every participant (6 observations per person) was determined and contrasted for person-level observations between Visual 3D and Nexus systems. Maximum, minimum, and range values were determined for each joint in all three planes of motion including foot progression angle associated with the left and right side as well as cadence, walking speed, step length, and stride length.

A paired t-test was performed comparing the mean values between the two systems. The associated p-value and confidence interval were determined when comparing the two systems. A p-value below 0.01 was used to determine significance in both parts of the analyses, (1) variance components models and (2) person-level analyses.

III. Results

III.A. Static and Dynamic Characterization

The results of the static linear testing are shown in Table 4. Markers placed at 57.5 mm represent the short foot distance. Those at 140.6 mm represent the long foot distance. For comparative purposes, t-test coefficients were chosen at the 0.05 and 0.01 levels of significance. Accuracy was noted in all three orientations for each distance with the greatest accuracy being in the Z-axis orientation followed by the Y and X for both the short and long foot distances. The mean accuracy from all five positions was 99.31%, 99.37%, and 99.64% for the X, Y, and Z orientations, respectively, for the short foot marker distance. The long foot marker distance had greater accuracy in all three orientations with values of 99.76%, 99.81%, and 99.90% for the X, Y, and Z orientations, respectively. The greatest resolution was shown in the short foot distance for all three orientations. The worst resolution was 0.63 ± 0.15 mm at the 0.05 level of significance for the long foot distance along the Y-orientation. The greatest resolution was 0.04 ±0.15 mm at the 0.05 level of significance for the short foot distance along the Z-orientation.

Table 4: Static accuracy and resolution results computed at the p = 0.05 and p = 0.01 level of significance.

Marker Distance	Orientation	Accuracy (%)	Resolution (mm)	P-Value
Short Foot (57.5 mm)	X-axis	99.31	0.17±0.15	0.05
			0.17±0.20	0.01
	Y-axis	99.37	0.31±0.15	0.05
			0.31±0.19	0.01
	Z-axis	99.64	0.04±0.15	0.05
			0.04±0.19	0.01
Long Foot (140.6 mm)	X-axis	99.76	0.52±0.15	0.05
			0.52±0.20	0.01
	Y-axis	99.81	0.63±0.15	0.05
			0.63±0.20	0.01
	Z-axis	99.90	0.35±0.15	0.05
			0.35±0.20	0.01

The results for the dynamic linear testing are shown in Table 5. The hip to knee marker distance displayed the highest accuracy of 99.77%. The lowest accuracy was seen at the short foot marker distance in the positive x-direction with 95.59%. The highest resolution was seen in the positive x-direction for the short foot marker distance with 0.05 ± 0.21 mm at the 0.05 level of significance. The worst resolution was seen in the negative x-direction for the long foot marker distance with 0.37 ± 0.30 mm at the 0.05 level of significance.

Table 5: Linear dynamic accuracy and resolution results computed at the p = 0.05 and p = 0.01 level of significance.

Marker Distance	Direction	Accuracy %	Resolution (mm)	P-Value
Short Foot (57.5 mm)	Forward (+X)	95.59	0.05±0.21	0.05
			0.05±0.27	0.01
	Backward (-X)	96.41	0.18±0.20	0.05
			0.18±0.26	0.01
Long Foot (140.6 mm)	Forward (+X)	96.89	0.25±0.23	0.05
			0.25±0.30	0.01
	Backward (-X)	97.08	0.37±0.23	0.05
			0.37±0.30	0.01
Hip to Mid-thigh (205.3mm)	Forward (+X)	99.46	0.31±0.23	0.05
			0.31±0.30	0.01
	Backward (-X)	99.54	0.33±0.21	0.05
			0.33±0.28	0.01
Hip to knee (417.8mm)	Forward (+X)	99.70	0.18±0.27	0.05
			0.18±0.35	0.01
	Backward (-X)	99.77	0.22±0.25	0.05
			0.22±0.33	0.01
Knee to Mid-calf (181.6mm)	Forward (+X)	99.37	0.25±0.21	0.05
			0.25±0.27	0.01
	Backward (-X)	99.27	0.13±0.21	0.05
			0.13±0.27	0.01
Knee to ankle (397.2mm)	Forward (+X)	99.61	0.13±0.26	0.05
			0.13±0.34	0.01
	Backward (-X)	99.60	0.09±0.26	0.05
			0.09±0.34	0.01

Table 6 depicts the resolution and accuracy results for the angular dynamic testing. The Biodex was programmed to rotate 90 degrees/second (representative gait

value). The planes of motion are included (XY, XZ, YZ).The range of motion was 305 degrees, but because of a ramp up and ramp down period for the Biodex, a 180 degree window of constant angular velocity in the middle of a 305-degree range at the center of each trial was used for analysis. The mean accuracy of the rotational dynamic testing was the highest with rotation in the XZ-plane (99.68%) for the hip to knee distance (417.8 mm). The lowest accuracy was seen in the XY-plane (94.82%) for the short foot distance (57.5 mm). The resolution was the greatest in the XZ-plane (0.10 ± 0.19) for the long foot distance (140.6 mm) at the 0.05 level of significance. The worst resolution was seen in the YZ-plane (0.61 ± 0.31 mm) at the 0.05 level of significance.

Table 6: Angular dynamic accuracy and resolution results computed at the p = 0.05 and p = 0.01 level of significance.

Marker Distance	Plane	Accuracy %	Resolution (mm)	P - Value
Short Foot (57.5 mm)	XY	94.82	0.38 ± 0.21	0.05
			0.38 ± 0.28	0.01
	XZ	98.21	0.27 ± 0.18	0.05
			0.27 ± 0.24	0.01
	YZ	97.17	0.27 ± 0.20	0.05
			0.27 ± 0.26	0.01
Long Foot (140.6 mm)	XY	97.89	0.18 ± 0.24	0.05
			0.18 ± 0.31	0.01
	XZ	99.04	0.10 ± 0.19	0.05
			0.10 ± 0.23	0.01
	YZ	98.43	0.28 ± 0.21	0.05
			0.28 ±0.28	0.01
Hip to midthigh (205.3mm)	XY	98.93	0.29 ± 0.25	0.05
			0.29 ± 0.33	0.01
	XZ	99.41	0.28 ± 0.22	0.05
			0.28 ± 0.29	0.01
	YZ	99.52	0.24 ± 0.23	0.05
			0.24 ± 0.30	0.01
Hip to knee (417.8mm)	XY	99.54	0.27 ± 0.27	0.05
			0.27 ± 0.36	0.01
	XZ	99.68	0.53 ± 0.29	0.05
			0.53 ± 0.38	0.01
	YZ	99.42	0.61 ± 0.31	0.05
			0.61 ± 0.41	0.01

III.B. Temporal and Stride Results

Temporal and stride parameters were broken up into left and ride side. Cadence, walking speed, step length, and stride length were determined using both Visual3D and Nexus softwares. Table 7 represents the average cadence, walking speed, step length and stride length for left and right sides of the body calculated from Visual3D and Nexus.

Table 7: Average cadence, walking speed, step length, and stride length for left and right side calculated from Visual3D and Nexus.

	Left		Right	
	Visual3D	Nexus	Visual3D	Nexus
Cadence (steps/min)	112.419	112.729	110.036	110.137
Walking Speed (m/s)	1.198	1.20	1.167	1.165
Step Length (m)	0.637	0.637	0.628	0.62
Stride Length (m)	1.281	1.278	1.250	1.269

Figures 7 and 8 are representations of an individual subject's average, male average, female average, and overall average for walking speed for both the right and left side of the body. Tables representing individual subject results, along with male averages, female averages, and overall averages for cadence, step length, and stride length for both right and left side can be found in Appendix E. Appendix F shows similar plots to that of figures 7 and 8 but with representation of cadence, step length, and stride length.

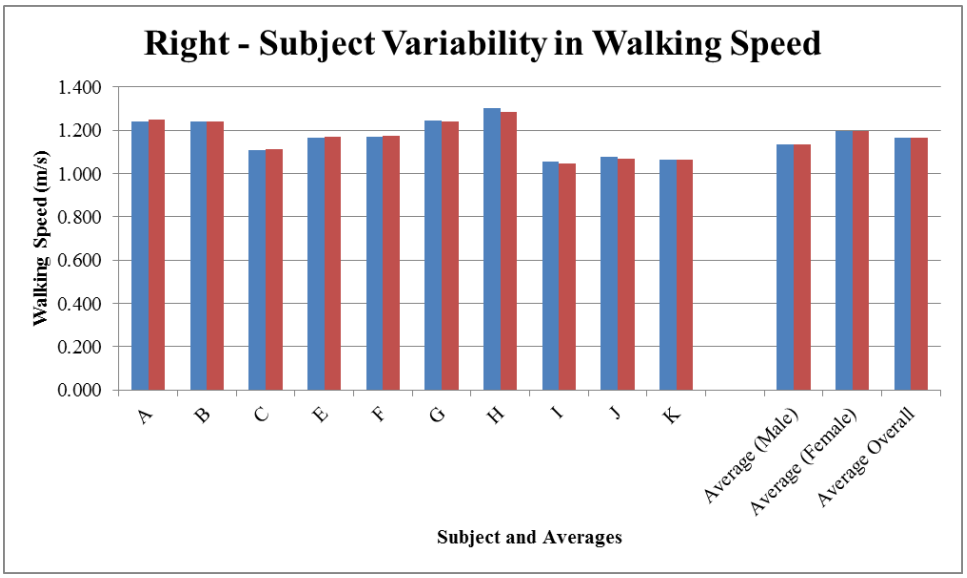

Figure 7: Right side walking speed variability between Visual3D and Nexus software. Blue represents Visual3D and red represents Nexus.

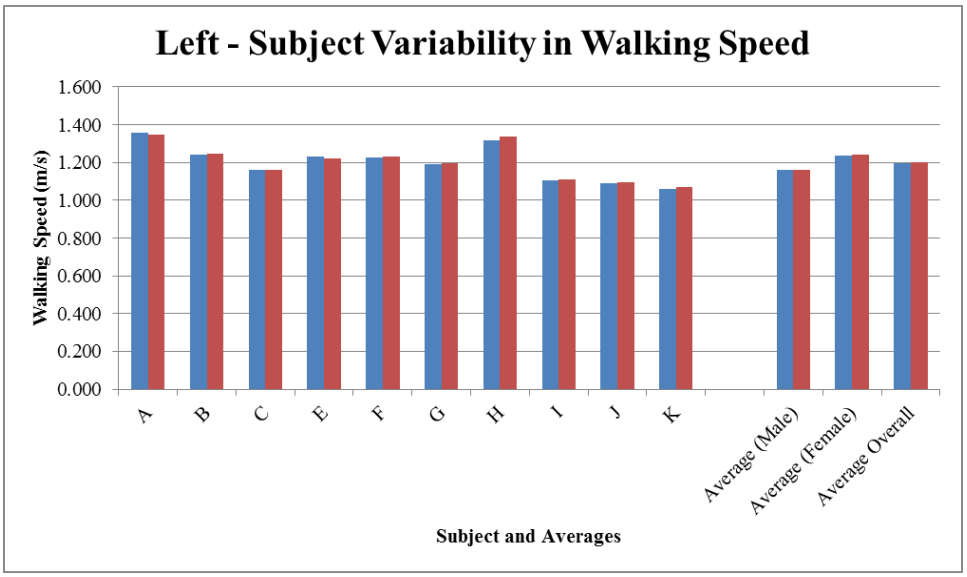

Figure 8: Left side walking speed variability between Visual3D and Nexus software. Blue represents Visual3D and red represents Nexus.

III.C. Kinematic Results

Figure 9A is a representation of the marker data recorded using AMASS and figure 9B represents that same marker data after it has been processed with the modified Helen-Hayes marker set through Visual3D. This particular trial is for subject B during one of the trials used for the left side. Figure 10 shows the joint angle data for the right knee. This is an example of the collaboration of all thirty trials, three trials from ten subjects, used for processing through Visual3D. The light blue area consists of ± 1 standard deviation. Joint angle data averages were calculated for the pelvis, hip, knee, and ankle in all three planes. The average joint angle maximum, minimum, and range were determined for four joints in three planes of motion for data processed through Visual3D and Nexus. The values were also calculated from the control subjects used in a study by Graf et al. The normal population was compared to a population with CTEV in the study [37]. For the purpose of this study, only the data from the normal population were used.

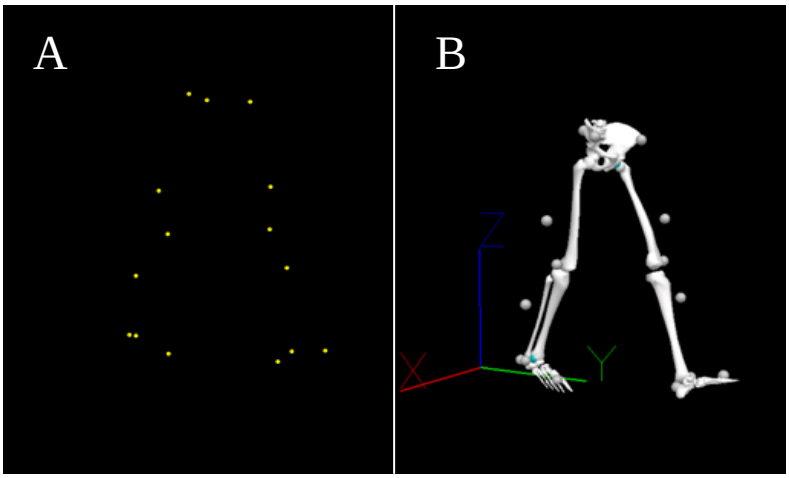

Figure 9: A) Marker data from AMASS processed and labeled. B) Marker data from AMASS processed through Visual3D using modified Helen-Hayes model.

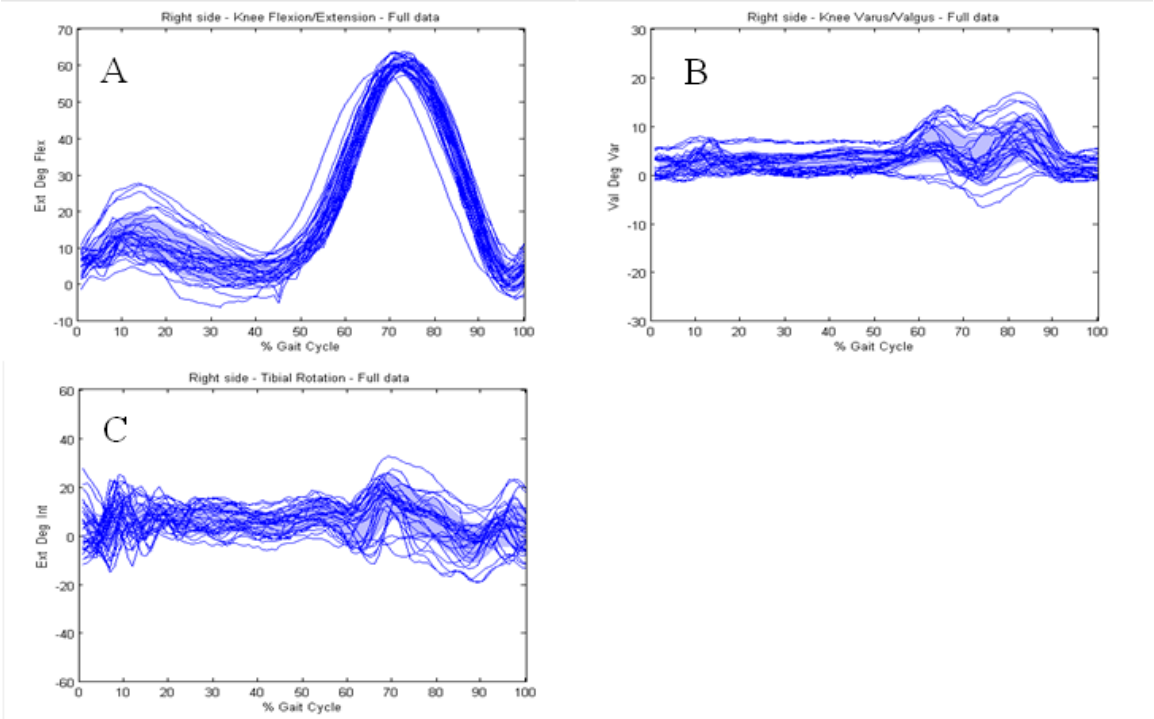

Figure 10: All thirty trials plotted with average and standard deviation for right side of knee processed with Visual3D. A) Knee flexion/extension, B) Knee valgus/varus, C) Tibial rotation.

The mean and standard deviation have been plotted for the entire gait cycle for both right and left side of the body after processing through Visual3D, Nexus, and clubfoot surgical release study controls. The five plots can be seen in Appendix H. Plots have also been created comparing the mean joint angle data for both Visual3D and Nexus and compared to the clubfoot study control data. Since the data was not separated into right and left side, the same set of data from the clubfoot study controls will be used for comparison with the right and left side of the data collected from Visual3D and Nexus. The graphs can be seen in Appendix I.

III.D. Comparative Results: Nexus vs.Visual3D

Figures 11 and 12 represent joint angle comparisons between Nexus and Visual3D for the left and right side, respectively. Each plot displays the mean and one standard deviation of the joint angle with respect to percent gait cycle. Nexus is represented by the solid blue line with light blue standard deviation and Visual3D is represented by the solid red line with the light red standard deviation. Any overlap between the two systems data will be shown in purple. When assessing both left and right sides, no significant deviation between the two sets of data was seen except in tibial rotation as well as each plot involving the foot. Table 8 represents the maximum, minimum, and range values shown for all of the joint angles where significant deviations were seen. A table showing the maximum, minimum, and range values for each joint on both sides can be seen in Appendix G.

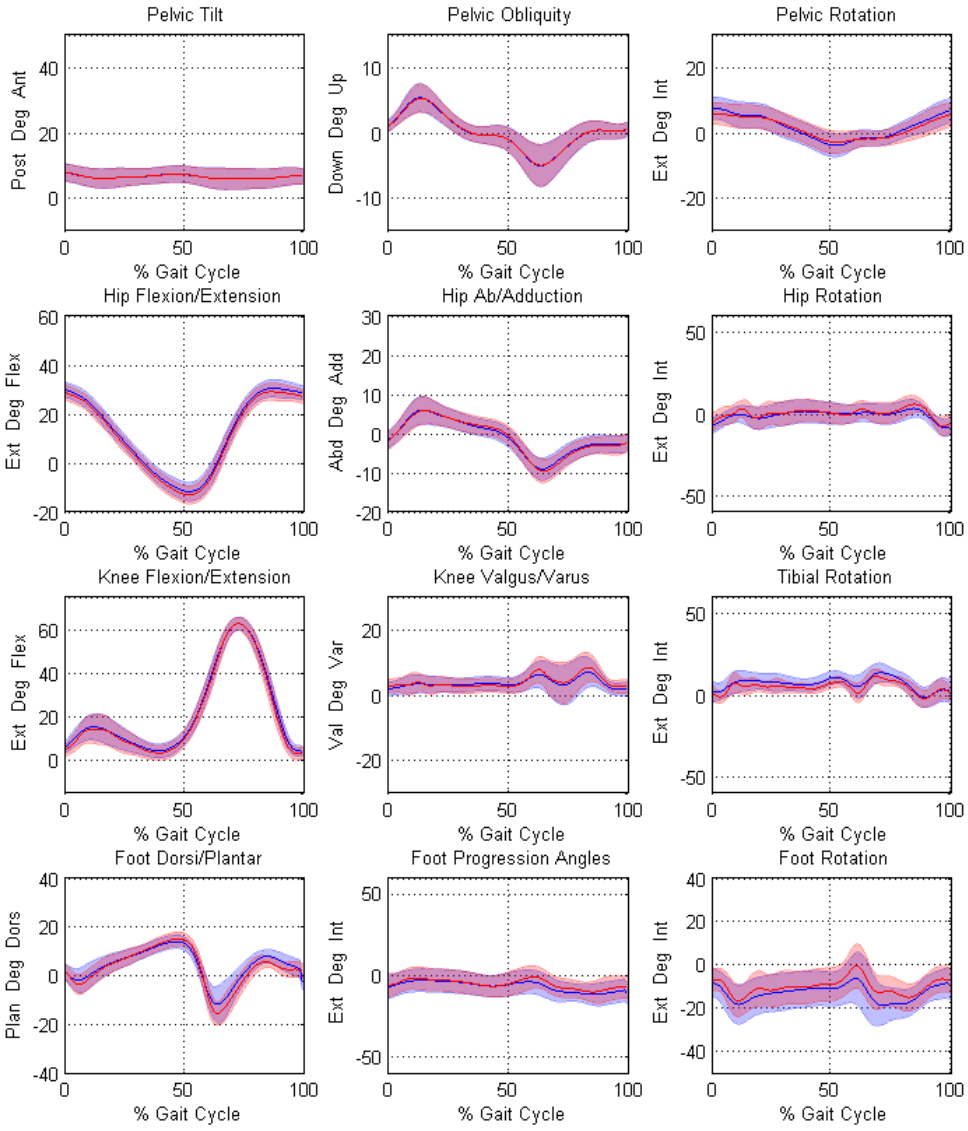

Figure 11: Left side - Visual3D and Nexus average and standard deviation joint angle data. Visual3D is blue and Nexus is red.

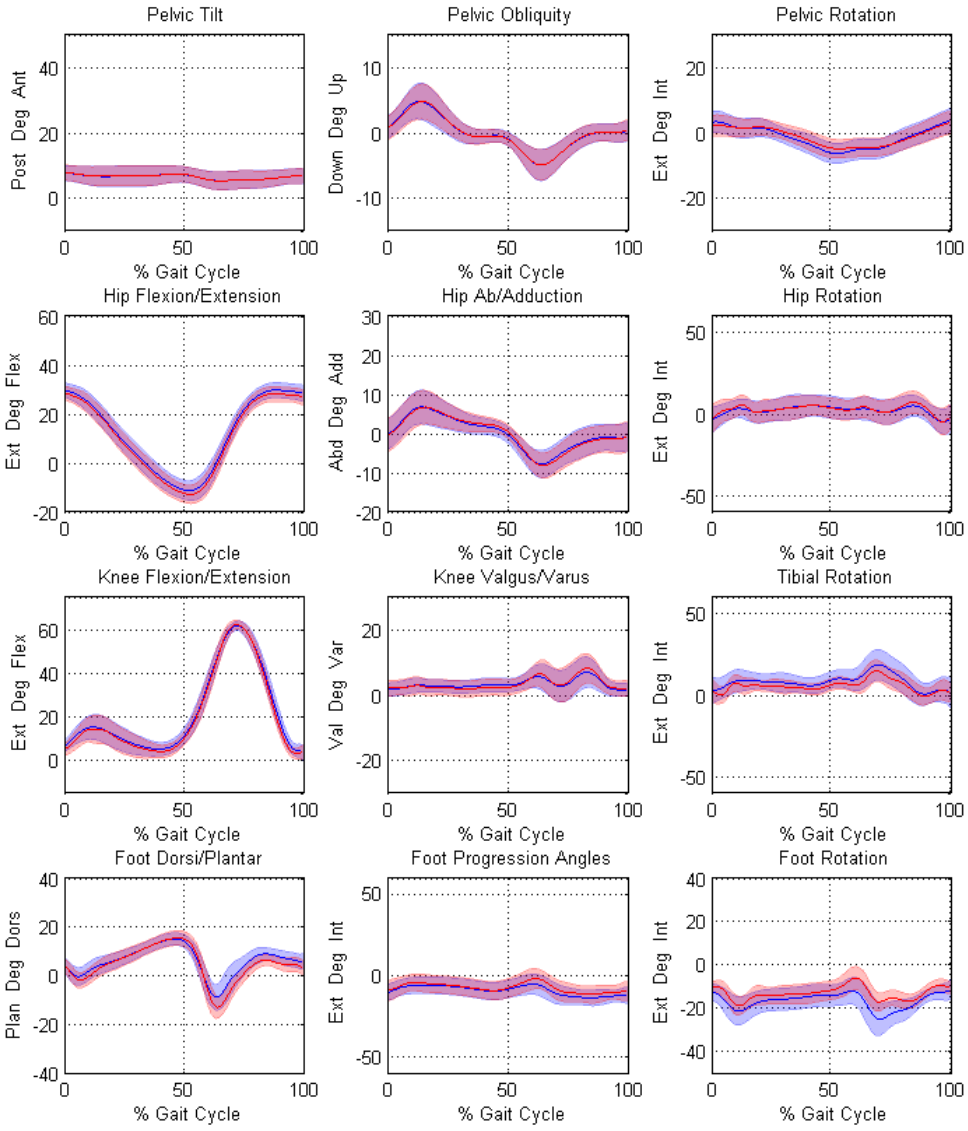

Figure 12: Right side - Visual3D and Nexus average and standard deviation joint angle data. Visual3D is blue and Nexus is red.

Table 8: Representation of the maximum, minimum, and range values associated with the joint angles where significant differences were seen between Visual3D and Nexus.

	Max			Min			Difference		
	Visual3D	Nexus	Control	Visual3D	Nexus	Control	Visual3D	Nexus	Control
Left Tibial Rotation	13.37	11.25	6.57						
Left Foot Dorsi Plantar	13.85	14.99	13.76	-11.64	-15.41	-11.30	25.49	30.40	25.06
Left Foot Progression	-2.74	-0.66	-3.17	-11.48	-9.88	-14.19	8.75	9.22	11.02
Left Foot Rotation	-6.22	-0.57	-3.93	-18.55	-16.55	-14.82			
Right Tibial Rotation	18.13	14.56	6.57						
Right Foot Dorsi Plantar	14.92	15.30	13.76	-8.78	-12.90	-11.30	23.71	28.21	25.06
Right Foot Progression	-5.16	-1.72	-3.17	-13.51	-11.43	-14.19	8.36	9.72	11.02
Right Foot Rotation	-11.31	-6.08	-3.93	-24.78	-18.69	-14.82			

III.E. Statistical Results

There are two portions of table 9. The first portion consists of the mean values for Nexus and Visual3D as well as the p-value associated with the variance of the calculated values due to the systems. The second portion deals with the overall difference between the mean values along with the standard deviation and the associated p-value which was determined from the paired t-test. Pelvic tilt, pelvic obliquity, pelvic rotation, hip flexion/extension, hip ab/adduction, hip rotation, knee flexion/extension, knee valgus/varus, cadence, walking speed, step length, and stride length showed no significant difference due to the systems and between average maximum, minimum, and range values. Tibial rotation maximum angle showed a significant difference in the variance due to the system with a p-value of 0.0042 but not with respect to the average difference between all of the values recorded with a p-value of 0.0295. The minimum and range values did not show any significant difference for tibial rotation. All of the joint angle values for the foot showed significant differences due to variance between the two systems as well as the average difference between the two systems overall. For foot dorsi/plantar flexion, the p-values associated with system variance were 0.0002, 0.0000, and 0.0000 for maximum, minimum, and range, respectively. The associated p-values from the paired t-test were 0.0021,

0.0051, and 0.0071 for maximum, minimum, and range, respectively. For foot progression angle, the p-values associated with system variance were 0.0000, 0.0005, and 0.0000 for maximum, minimum, and range, respectively. The associated p-values from the paired t-test were 0.0001, 0.0001, and 0.0004 for maximum, minimum, and range, respectively.

Table 9: Mean values for Nexus and Visual3D for maximum, minimum, and range for each joint angle. System P-value represents variance with respect to measurement differences between systems. Delta and Delta P-value represent differences between overall mean values as well as significance of overall difference. P-value less than 0.01 represents a significant difference.

Parameter		Mean (Nexus)	Mean (Visual3d)	System P-value	Delta (Nexus - Visual3d)	Delta P-Value
Pelvic Tilt	Max Angle	8.2600	8.2347	1.0000	0.0253 ± 1.8780	0.9669
	Min Angle	4.7979	4.7396	1.0000	0.0585 ± 1.8000	0.9209
	Range	3.4620	3.4951	1.0000	-0.0330 ± 0.6263	0.8707
Pelvic Obliquity	Max Angle	5.0857	5.1091	1.0000	-0.0234 ± 1.0359	0.9446
	Min Angle	-5.0778	-5.0881	1.0000	0.0103 ± 1.2353	0.9796
	Range	10.1635	10.1972	1.0000	-0.0337 ± 2.1297	0.9612
Pelvic Rotation	Max Angle	5.3012	5.8928	0.5240	-0.5917 ± 1.8643	0.3418
	Min Angle	-4.6873	-5.0756	0.9541	0.3882 ± 1.4457	0.4178
	Range	9.9885	10.9684	0.1761	-0.9799 ± 2.0541	0.1657
Hip Flexion/ Extension	Max Angle	29.6827	30.3139	0.2702	-0.6312 ± 1.5289	0.2241
	Min Angle	-13.1697	-12.2398	0.2670	-0.9299 ± 3.2141	0.3841
	Range	42.8524	42.5537	0.9997	0.2987 ± 2.5332	0.7179
Hip Ab/Adduction	Max Angle	6.4850	6.4620	1.0000	0.0230 ± 1.6067	0.9650
	Min Angle	-9.2297	-8.8870	1.0000	-0.3427 ± 1.8157	0.5653
	Range	15.7147	15.3490	0.9998	0.3657 ± 2.3671	0.6369
Hip Rotation	Max Angle	8.8225	7.8896	0.3839	0.9330 ± 3.0127	0.3530
	Min Angle	-8.6097	-8.4509	0.9997	-0.1588 ± 2.3478	0.8354
	Range	17.4323	16.3405	0.0516	1.0918 ±1.8896	0.1010
Knee Flexion/ Extension	Max Angle	62.5908	62.3278	0.9998	0.2631 ± 1.5230	0.5982
	Min Angle	1.5143	2.2998	0.1714	-0.7855 ± 1.9790	0.2411
	Range	61.0765	60.0280	0.0947	1.0485 ± 1.9331	0.1204
Knee Valgus/ Varus	Max Angle	9.5962	9.1508	0.7162	0.4454 ± 1.808	0.4560
	Min Angle	-0.5641	-0.6119	1.0000	0.0478 ± 2.0455	0.9428
	Range	10.1603	9.7627	0.9290	0.3976 ± 1.6561	0.4671
Tibial Rotation	Max Angle	15.2345	17.2448	0.0042	-2.0102 ± 2.4596	0.0295
	Min Angle	-5.1418	-4.6312	0.8523	-0.5106 ± 1.4132	0.2827
	Range	20.3763	21.8759	0.1023	-1.4996 ± 3.1281	0.1638
Foot Dorsi/ Plantar	Max Angle	15.4928	14.6275	0.0002	0.8653 ±0.6421	0.0021
	Min Angle	-15.2394	-11.0812	0.0000	-4.1582 ± 3.5734	0.0051
	Range	30.7322	25.7087	0.0000	5.0235 ± 3.6152	0.0017
Foot Progression Angles	Max Angle	0.6479	-2.1120	0.0000	2.7600 ± 1.2542	0.0001
	Min Angle	-13.5850	-15.1884	0.0005	1.6034 ± 0.7043	0.0001
	Range	14.2329	19.5126	0.0000	5.2797 ± 3.0050	0.0004
Foot Rotation	Max Angle	-1.8645	-6.2080	0.0000	4.3434 ± 1.8491	0.0000
	Min Angle	-19.9750	-24.7497	0.0000	4.7747 ± 4.1952	0.0058
	Range	18.1105	18.5417	1.0000	0.4313 ± 3.9345	0.7368
Cadence		111.4642	111.2274	1.0000	0.2368 ± 1.1886	0.5443
Walking Speed		1.1827	1.1822	1.0000	0.0005 ± 0.0031	0.6312
Step Length		0.6287	0.6323	0.8932	-0.0037 ± 0.0043	0.2530
Stride Length		1.2737	1.2655	1.0000	0.0081 ± 0.0297	0.4078

For foot rotation, only the maximum and minimum angles showed a significant difference due to the system. The p-values associated with system variance were 0.0000 for both maximum and minimum. The range had a p-value of 1.0000 which means there is no difference seen between the two systems. The associated p-values for the paired t-test were 0.0004 and 0.0000 for maximum and minimum, respectively. The range p-value was 0.7368 for the paired t-test.

IV. Discussion

IV.A. System Characterization

Error in marker location was reduced through standard camera linearization, which accounts for the distortion due to the curvature of the camera lens [38]. This process also helps reduce marker dropout. Optitrack ARENA software is able to export marker locus data using C3D files. For the calibration trials, a rigid body with labels for each marker is defined to check the data format for export. This allows proper expedited data formation, minimal marker dropout, and reduced number of false markers seen by the system.

The static calibration trials provided comparable results to those reported in studies with Vicon motion tracking systems. Kidder et al. obtained static and dynamic results using a five-camera Vicon motion tracking system. Results showed static accuracy and resolution with a minimum of 99.4% accuracy and 0.6 ± 0.82 mm at the 0.05 level of significance. [27]. Myers et al. used a fifteen-camera Vicon 524 motion tracking system and performed similar static and dynamic trials with comparable results. Static testing produced a minimum accuracy of 99.88% and resolution of 0.60 ± 0.14 mm at the 0.05 level of significance [28]. The results obtained from the Optitrack motion tracking system provide results similar to those of Kidder and Myers with a minimum accuracy of 99.31% and resolution of 0.63 ± 0.15 mm at the 0.05 level of significance.

Angular dynamic trials were reported by Kidder et al. with a minimum accuracy of 98.3% and resolution of 1.49 ± 0.10 mm at the 0.05 level of significance [28]. Myers et al. performed both linear and angular dynamic trials. The linear dynamic trials resulted in a minimum accuracy of 99.81% and resolution of 0.53 ± 0.18 mm at the 0.05 level of significance. The angular dynamic trials had a minimum accuracy of 99.18% and a resolution of 2.96 ± 3.53 mm [27]. The linear dynamic trials for the Optitrack system had a minimum accuracy of 95.59% and resolution of 0.37 ± 0.23 mm at the 0.05 level of significance. The angular dynamic trials had a minimum accuracy of 94.82% and resolution of 0.61 ± 0.31 mm at the 0.05 level of significance.

Optitrack's minimum accuracy is less than that reported in similar Vicon studies. The Myers et al. study used fifteen cameras which can significantly increase the accuracy of the marker location since there are more redundant cameras used in determining the 3-D location of each marker. The prudent use of additional cameras in the Optitrack configuration is an option to increase accuracy when necessary.

In the Myers et al. study, the minimal marker distance was 39.9 mm, whereas the distance was increased to 57.5 mm for the Optitrack system [27]. This finding helps define the limits of application for the Optitrack system with an eight-camera configuration. This would support use of the multi-segmental foot models but restrict use to adolescents or adults. Other marker distances produce accuracy percentages at levels close to those reported for the Vicon system. These include the whole body gait models, walker and crutch models, and wheelchair models for both adult and pediatric applications.

The resolution throughout all of the validation trials was comparable to those reported in other studies [27, 28]. The values were less than that of similar VICON studies. These results also support further use of the Optitrack system for adult and pediatric motion analysis applications [62]. By increasing the number of cameras used and each camera's pixel value, the resolution and accuracy can increase and its potential applications would increase.

It is very important that the resolution and accuracy of the system are reliable in that deviations from the true values can have dramatic offsets for kinematic and kinetic values. A study by Stagni et al. found that if the hip joint center were calculated with an anterior mislocation of 30 mm, then the flexion/extension moment had a 22% error. With a 30 mm lateral mislocation, there was an abduction/adduction error of 15%. This is showing that a subtle difference with the information calculated from the marker data can result in a dramatic difference in values seen in kinematics and kinetics from what they truly are [69]. Since joint centers are calculated from marker data, such as the hip, knee, and ankle, it is important that the marker locations recorded are accurate. This can be affected by camera position, what kind of view the cameras have on the markers, pixel value, and number of cameras. All of these can impart the results that are obtained. With advancements in technology and cost of equipment, it will become easier to get accurate and reliable data.

IV.B. Kinematic Findings

Within each software system, coordinate axes and segments are created to determine joint angle kinematics. When looking at the big picture, the two systems provide very similar data which can be noted in the results. Starting with the pelvis, no significant differences were seen at the maximum, minimum, and range values for all three planes of motion. The same can be said for both the hip and the knee except for the maximum angle associated with tibial rotation. This difference may be explained by the fact that the models used in Visual3D and Nexus utilize tibial rotation differently along with the references they use for the tibial segment coordinate orientations. Visual3D uses the ankle marker and Nexus uses the calculated ankle joint center. This could cause differences in the axes directions causing a subtle difference in the maximum angle for tibial rotation. Significant differences were seen at the ankle joint with the exception of

the range value for foot rotation. This can be explained because of differences in the foot segment coordinate system used in the model, which will be discussed later. It was also seen that temporal and stride parameters showed no significant differences. This means that step length, stride length, cadence, and walking speed were the same when compared between software systems. Overall, the majority of values compared showed no significant differences due to the two different systems being used. This is beneficial when trying to apply the less expensive system to real world applications.

There are a number of reasons that discrepancies can be seen within values between the two systems, even though the same marker files were processed through each system. One of the biggest differences is due to the difference is pose estimation algorithms used. Nexus uses a Direct Pose Estimation or Global Optimization (OLGA) while Visual3D uses Segment Optimization or Global Optimization [60, 61]. These are two methods for interpreting joint angles where there was marker drop out. The differences could potentially cause maximum and minimum values to vary between trials. Another source for error for all of the joint angles is due to the selection of foot strike and foot off. Determining foot strike and foot off can be challenging without the use of a force plate since you cannot determine the point at which a force can be recorded. In order to compensate for this issue, the foot strike and foot off had to be determined manually for both Nexus and Visual3D. Nexus software allows for the individual tracking of markers. Thus, it was easier to determine foot strike and foot off because the path of the marker was followed. For foot strike, the heel marker was tracked and the point when the marker no longer moved forward was marked as foot strike. For foot off, the metatarsal marker was tracked and the point when forward movement of the marker

was initiated was marked as foot off. The same process was performed for Visual3D but since there was no line that follows the path of each marker, an estimation of which frame was associated with foot strike and foot off was used. Since there was noise in the signal of the markers location, a frame could have been interpreted as moving when it was not or not moving when it was. From this, different frames could have been selected for the same foot strike or foot off between the two systems. The main values that this issue would affect would be the temporal and stride parameters, but from looking at the results, it was not a large issue.

Filtering could also account for some discrepancies between the two systems. Filtering is optional for both systems but it is encouraged to utilize this feature since the data is typically easier to interpret after being filtered. Visual3D uses a 6 Hz Butterworth filter with the number of samples reflected as six, total number of samples in the Buffer as six, and the number of bidirectional passes as one. Nexus used a Woltring filter which utilizes spline smoothing and is equivalent to a double Butterworth filter [63]. The mean squared error and general cross validation are used to choose a noise level with which to filter the data. This discrepancy between the two filters applied to the joint angle data may account for some of the differences. Since the two filtering methods are almost equivalent, this should only contribute a minor portion to any differences seen. A sample of three trials taken from subject A is plotted in figure 13. This sample consists of joint angle data from the knee where the trials were not filtered for both Visual3D and Nexus. It can be seen that even when the data is not filtered, there is still consistency in the patterns between the output of Visual3D and Nexus. There are some subtle differences but, typically, there is less than a degree of difference between the patterns.

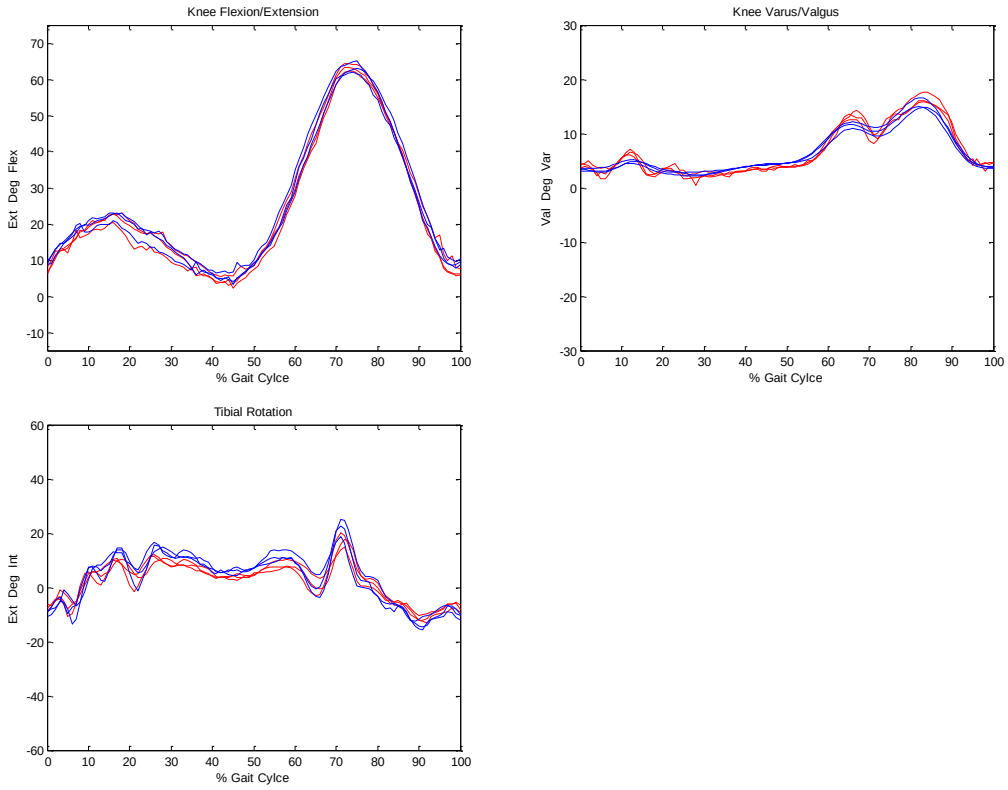

Figure 13: Plot of three trials from subject A for the knee with the data unfiltered. Red is Visual3D and blue is Nexus.

The main discrepancies found within the maximum, minimum, and range values for the joint angles can be accounted for by the differences seen in the coordinate axes used for the foot segment. Figure 14 is a representation of the foot segment coordinate system for both Nexus and Visual3D. Visual3D is represented by the solid lines and Nexus is represented by the dashed lines. The segment coordinate system for Visual3D is first created by a line from the heel marker to the toe marker. This line is known as the primary axis which will be used for coronal plane motion. The secondary axis is created by a line from the heel to a landmark created directly inferior to the heel marker, represented by the R_HEEL_Z landmark. This line is known as the secondary axis and will be used for motion in the transverse plane. The final axis is orthogonal to both the

primary and secondary axis and points to the right. This will be used to describe sagittal plane motion. For the foot segment created in Nexus, two initial segments are created. The first foot segment, represented by figure 15A, uses a TOE-HEE line as its primary axis taken as the Y-axis. The direction of the X-axis from the untortioned tibia used to define the secondary y-axis. The Z-axis points down and the X-axis points to the left. The second foot segment, figure 15B, uses the TOE-AJC (ankle joint center to metatarsal marker) as the primary axis. The Y-axis of the untortioned tibia is used to define the perpendicular X-axis and the foot Z-axis. The plantar flexion offset and rotation offset seen in figure 15C are then calculated. The plantar flexion offset is taken from the rotation around the X-axis, and the rotation offset is taken around the Z-axis and the angle around the Y-axis is ignored. The coordinate system for Vicon's foot segment is centered at the ankle joint center. The rotation offset is based off of two lines. One is created from the heel to the toe marker while the other is taken from the ankle joint center to the toe marker. The coordinate system is then rotated about the vertical axis by the angle created between these two lines. This can explain part of the differences seen between the two systems since one rotation about an axis can affect the other two axes.

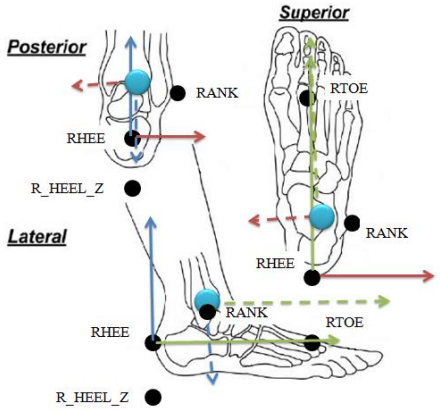

Figure 14: Representation of the foot segment created in Visual3D and Nexus. Visual3D and Nexus are represented by solid and dashed lines, respectively. The blue circle represents the ankle joint center.

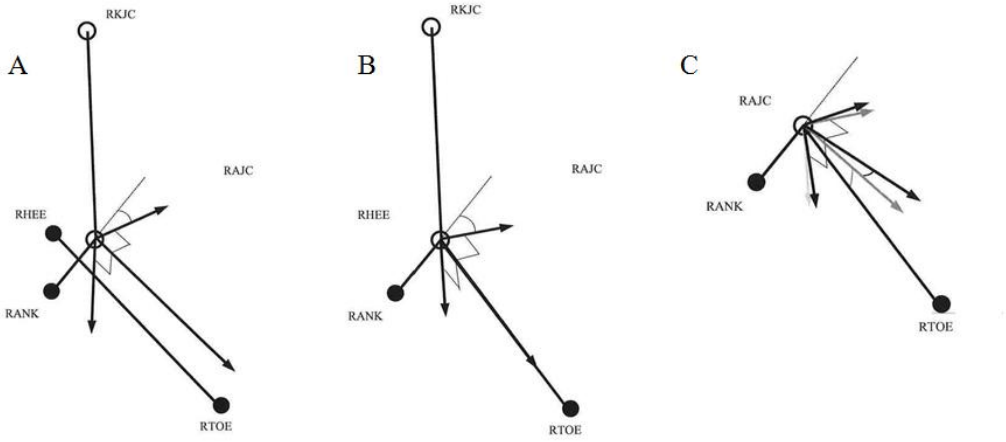

Figure 15: A) Main foot segment constructed using the TOE-HEE line as primary axis (Y), direction of untortioned tibia used for secondary axis (X), and tertiary axis points down (Z). B) Second foot segment using TOE-AJC as primary axis (Y), untorsioned tibia to define secondary axis (X), and tertiary axis points down (Z). C) Corrected foot segment accounting for plantar flexion offset and rotation offset [67].

Another concern is the coordinate system center is located at the ankle joint center for the Nexus system and is located at the heel for the Visual3D system. An axis line that is parallel to a line created from the heel to toe marker is needed but the origin of that line

needs to be at the ankle joint center. This is where the plantar flexion offset comes into play. Visual3D cannot account for this offset set in order to create something similar, a line is created from the heel to toe marker but the center of the coordinate system is located at the heel as opposed to the ankle joint center. Also, the x-axis in the Vicon system may not be oriented directly in the vertical direction (Figure 15C). This is different than the vertical axis used in Visual3D which does not have any offset from a purely vertical direction. This subtle offset that may occur between the two systems can account for differences seen in the foot progression angle and foot rotation results. The rotation offset from the tibia and ankle marker can account for possible changes in sagittal plane motion between the two systems, which can be seen in the foot dorsi/plantar flexion plots. The differences seen between Visual3D and Vicon's foot segment coordinate system, including coordinate axis orientation, foot strike and foot off frame selection, gap interpolation, and filtering can all account for the significant difference seen in the results. Even with all of these differences, the overall result is very promising. A majority of the values compared showed no significant difference and provided the same results for both systems.

There was also a qualitative comparison done with a study comparing control subjects (normal) to those with clubfoot [37]. Figures 27 (left side) and 28 (right side) in Appendix I show the plots of the mean joint angle data for Nexus and Visual3D compared with that of ±1 standard deviation data from the clubfoot study. For the left side, the mean plots created by both systems are within the boundaries for the data from the clubfoot study. Some of the plots on the left side are close to the end of the standard deviation plots such as pelvic rotation, hip ab/adduction, knee flexion/extension, knee

valgus/varus, and tibial rotation. On the right side, a similar trend is seen except that two of the plots have Visual3D results reaching outside of the standard deviation window which include tibial rotation and foot rotation. This can be explained again since the foot models are different between Nexus and Visual3D.

IV. C. Future Applications

With the validation of the motion analysis system, several directions can be followed in order to expand the use of the system. The first step would be to create multi-segmental foot and upper extremity models [2, 15] within Visual3D for easy use by clinicians and researchers. With these models created in Visual3D, several new populations of subjects can be analyzed and treated using an inexpensive system for analysis consisting of the Optitrack cameras and Visual3D software. Since the foot is composed of many bones and should not be thought of as a single rigid body, it is important to apply a model that accounts for this variability. This is where a multi-segmental foot model comes in. With the use of an inexpensive system, the number of people and clinics where it can be used may increase dramatically. The same concept can be said for people in wheelchairs and crutches with the use of the upper extremity model. Other future directions would include purchasing more cameras and mounts to ensure the maximum potential of the cameras is being used. It is important to have the cameras high enough to provide a large enough field of view. With the increased number of cameras used in the system, the resolution and accuracy can be increased. This will also benefit if the number of megapixels used increases. For example, the Flex 13 cameras offered by Naturalpoint, Inc. offer 1.3 megapixels as opposed to the V100:R2 cameras with only 0.3 megapixels with just a $400/camera increase in price. With an increase in camera

resolution and accuracy, the possible populations for gait analysis may increase since markers can be placed closer together. This would allow for analysis, such as pediatric ankle and foot models, to be characterized since it might be limited with the system used in this study. Also, in order to provide full gait analysis, force plates will be added and a walkway will be built to calculate joint kinetics. EMG electrodes will also be added to determine muscle activity. All of this will further expand the capabilities of the system being developed.

V. Conclusion

The Optitrack motion capture cameras have been evaluated through static, linear dynamic, and angular dynamic calibrations. The results are supportive of further testing and potential application in pediatric and adult motion analysis. With the use of these cameras and Visual3D biomechanics modeling software, joint angle data were compared to that of data analyzed using Nexus 1.7 software from Vicon, currently a clinical standard. Results showed that the joint angle maximum, minimum, and range values are not significantly different due to system processing for the pelvis, hip, and the entire knee, expect for the maximum angle for tibial rotation. There were significant differences due to system variability for the entire ankle except for the foot rotation range value. This can be explained because of the variance in coordinate systems used for the foot segment in the two systems. Validation of the Optitrack and Visual3D system is a first step towards expansion of motion analysis to a broader clinical community. Kinetic application will require incorporation of force plates and EMG data synchronized to the existing kinematic system. With Optitrack, expansion of new camera configurations is an affordable option. The available Visual3D software offers many model options including

the Helen Hayes, Oxford foot, and upper extremity models, as well as models the user can create incorporate. This may be attractive for future clinical and research applications.

BIBLIOGRAPHY

[1] Freeman, Miller. Cerebral Palsy. New York, NY: 2005. Print.

[2] Slavens BA, Sturm PF, Bajournaite R, Harris GF. Upper Extremity Dynamics during Lofstrand Crutch-Assisted Gait in Children with Myelomeningocele. Gait and Posture 2009; 30:511-517.

[3] Strifling KM, Lu N, Wang M, Cao K, Ackman JD, Klein JP, Schwab JP, Harris GF. Comparison of Upper Extremity Kinematics in Children with Spastic Diplegic Cerebral Palsy Using Anterior and Posterior Walkers. Gait and Posture 2008; 28:412-419.

[4] Konop K, Strifling K, Wang M, Cao K, Eastwood D, Jackson S, Ackman J, Schwab J, Harris GF. A Biomechanical Analysis of Upper Extremity Kinetics in Children with Cerebral Palsy using Anterior and Posterior Walkers. Gait and Posture 2009; 30:364-369.

[5] Hingtgen B, Wang M, McGuire J, Harris GF. An upper extremity model for evaluating of hemiparetic stroke. Journal of Biomechanics 2006; 39(4):681-688.

[6] Cooper RA. Biomechanics of Mobility and Manipulation. Rehabilitation Engineering: Applied to Mobility and Manipulation. Philadelphia: IOP Publishing Ltd: 1995:69-154.

[7] Kadaba MP, Ramakrishnan HK, Wootten ME Measurement of Lower Extremity Kinematics during Level Walking. Journal of Orthopaedic Research 1990; 8:383-392.

[8] Davis III RB, Ounpuu S, Tyburski D, Gage JR. A gait analysis data collection and reduction technique. Human Movement Science 1991; 10:575-587.

[9] Gage JR, Novacheck TF. An Update on the Treatment of Gait Problems in Cerebral Palsy. Journal of Pediatric Orthopaedics 2001; 10:265-274.

[10] Wiley ME, Damiano DL. Lower-extremity strength profiles in spastic cerebral palsy. Developmental Medicine & Child Neurology 1998; 40:100-107.

[11] Gutierrez GM, Chow JW, Tillman MD, McCoy SC, Castellano V, White LJ. Resistance Training improves gait kinematics in Persons with Multiple Sclerosis. Archives of Physical Medicine and Rehabilitation 2005; 86:1824-1829.

[12] El-Hawary R, Karol LA, Jeans KA, Richards BS. Gait Analysis of Children Treated for Clubfoot with Physical Therapy or the Ponseti Cast Technique. Journal of Bone and Joint Surgery 2008; 90(7):1508-1516.

[13] Fritz JM, Guan Y, Wang M, Smith PA, Harris GF. A Fracture Risk Assessment Model of the Femur in Children with Osteogenesis Imperfecta (OI) during Gait. Medical Engineering and Physics 2009; 31:1043-1048.

[14] Davids JR, Huskamp M, Bagley AM. A Dynamic Biomechanical Analysis of the Etiology of Adolescent Tibia Vara. Journal of Pediatric Orthopaedics 1996; 16(4):461-468.

[15] Rankine L, Long J, Canseco K, Harris GF. Multisegmental Foot Modeling: A Review. Critical Reviews in Biomedical Engineering 2008; 36(2-3):127-181.

[16] Canseco K, Rankine L, Long J, Smedburg T, Marks R, Harris GF. Motion of the Multisegmental Foot in Hallux Valgus. Foot and Ankle International 2010; 31(2):146-152.

[17] Canseco K, Long J, Marks R, Khazzam M, Harris GF. Quantitative Characterization of Gait Kinematics in Patients with Hallux Rigidus Using the Milwaukee Foot Model. Journal of Orthopaedic Research 2008; 26:419-427.

[18] Canseco K, Long J, Marks R, Khazzam M, Harris GF. Quantitative Motion Analysis in Patients with Hallux Rigidus before and after Cheilectomy. Journal of Orthopaedic Research 2009; 27:128-134.

[19] Marks RM, Long JT, Ness ME, Khazzam M, Harris GF. Surgical Reconstruction of Posterior Tibial Tendon Dysfunction: Prospective Comparison of Flexor Digitorum Longus Substitution Combined with Lateral Column Lengthening or Medial Displacement Calcaneal Osteotomy. Gait and Posture 2009; 29:17-22.

[20] Myers KA, Long JT, Klein JP, Wertsch JJ, Janisse D, Harris GF. Biomechanical implications of the negative heel rocker sole shoe: Gait kinematics and kinetics. Gait and Posture 2006; 24:323-330.

[21] Long JT, Klein JP, Wertsch JJ, Janisse D, Sirota NM, Harris GF. Biomechanics of the Double Rocker Sole Shoe: Gait Kinematics and Kinetics. Journal of Biomechanics 2007; 40:2882-2890.

[22] Graf A, Hassani S, Krzak J, Caudill A, Flanagan A, Bajorunaite R, Harris G, Smith P. Gait Characteristics and Functional Assessment of Children with Type I Osteogenesis Imperfecta. Journal of Orthopaedic Research 2009; 27:1182-1190.

[23] "Gait Analysis Rehabilitation." *Vicon.* Web. 3 Jan 2012. <http://www.vicon.com/applications/gait_analysis.html>.

[24] “Optotrak Certus Motion Capture System.” *Northern Digital Inc*. Web. 3 Jan 2012. <http://www.ndigital.com/lifesciences/certus-software.php>.

[25] "Gait Analysis." *Motion Analysis: The Industry Leader for 3D Passive Optical Motion Capture*. Web. 3 Jan 2012. <http://www.motionanalysis.com/html/movement/gait.html>.

[26] "3D Biomechanics Research Software – Visual3D™." *C-Motion Research Biomechanics*. Web. 3 Jan 2012. <http://www.c-motion.com>

[27] Myers KA, Wang M, Marks RM, Harris GF. Validation of a Multisegment Foot and Ankle Kinematic Model for Pediatric Gait. IEEE/TNSRE 2004; 12(1):122-130.

[28] Kidder SM, Abuzzahab FS, Harris GF, Johnson JE. A system for the analysis of foot and ankle kinematics during gait IEEE/TNSRE 1996; 4:25-32.

[29] Schmidt J, Berg DR, Ploeg HL. Precision, repeatability and accuracy of Optotrak optical motion track systems. International Journal of Experimental and Computational Biomechanics 2009; 1(1):114-127.

[30] Kadaba MP, Wooten ME, Ramakrishnan HK, Hurwitz D, Cochran GV. Assessment of human motion with VICON. ASME Biomechanical Symposium 1989; 84:335-338.

[31] Van den Bogart AJ, Smith GD, Nigg BM. *In vivo* determination of the anatomical axes of the ankle joint complex: An optimization approach. Journal of Biomechanics 1994; 27(12):1477-1488.

[32] Veeger HE, Yu B, An K, Rozendal RH. Parameters for Modeling the Upper Extremity. Journal of Biomechanics 1997; 30(6):647-652.

[33] Nachtigal CH. Instrumentation and Control: Fundamentals and Applications. New York: Wiley, p. 62, 1990.

[34] Schwartz MH, Rozumalski A, Trost JP. The effects of walking speed on the gait of typically developing children. Journal of Biomechanics 2008; 41:1639-1650.

[35] Post DC. Gait Analysis Review. 2006. <http://www.nd.edu/~dpost/IntSyst/report1.pdf>

[36] Krzak JJ, Graf A, Flanagan A, Caudill A, Smith P, Harris GF. Analysis of Push-Off during Locomotion in Children with Type 1 Osteogenesis Imperfecta. Journal of Experimental and Clinical Medicine 2011; 3(5):195-199.

[37] Graf A, Hassani S, Krzak J, Long J, Caudill A, Flanagan A, Eastwood D, Kuo K, Harris G, Smith P. Long-Term Outcome Evaluation in Young Adults Following Clubfoot Surgical Release. Journal of Pediatric Orthopaedics 2010; 30(4): 379-385.

[38] Board M. Telephone interview. 14 June 2011.

[39] Leo KH, Tan BY. User-tracking mobile floor projection virtual reality game system for paediatric gait. iCREATe 2010; 25:1-4.

[40] Zhang S, Leo KH. A Hybrid Human Motion Tracking System for Virtual Rehabilitation. IEEE Industrial Electronics and Applications 2011; 6:1993-1998.

[41] Watanabe Y, Hatanaka T, Komuro T, Ishikawa M. Human Gait Estimation Using a Wearable Camera. IEEE Applications of Computer Vision 2010; 2:276-281.

[42] Jaspers E, Feys H, Bruyninckx H, Cutti A, Harlaar J, Molenaers G, Desloovere K. The reliability of upper limb kinematics in children with hemiplegic cerebral palsy. Gait and Posture 2011; 33(4): 568-576.

[43] Elliot C, Reid S, Hamer P, Alderson J, Elliott B. Lycra® arm splints improve movement fluency in children with cerebral palsy. Gait and Posture 2011; 33(2): 214-219.

[44] Reid S, Elliot C, Alderson J, Lloyd D, Elliot B. Repeatability of upper limb kinematics for children with and without cerebral palsy. Gait and Posture 2010; 32(1): 10-17.

[45] Buczek F, Sinsel EW, Gloekler DS, Wimer BM, Warren CM, Wu JZ. Kinematic performance of a six degree-of-freedom hand model (6DHand) for use in occupational biomechanics. Journal of Biomechanics 2011; 44(9): 1805-1809.

[46] Kobayashi T, Leung A, Akazawa Y, Hutchins S. Design of a stiffness-adjustable ankle-foot orthosis and its effects on ankle joint kinematics in patients with stroke. Gait and Posture 2011 33(4): 721-723.

[47] Tulchin K, Orendurff M, Karol L. A comparison of multi-segment foot kinematics during level overground and treadmill walking. Gait and Posture 2010; 31(1): 104-108.

[48] Dubbeldam R, Nene A, Buurke J, Groothuis-Oudshoorn C, Baan H, Drossaers-Bakker K, van de Laar M, Hermens H. Foot and ankle joint kinematics in rheumatoid arthritis cannot only be explained by alteration in walking speed. Gait and Posture 2011; 33(3): 390-395.

[49] Wang R, Gutierrez-Farewik E. The effect of subtalar inversion/eversion on the dynamic function of the tibialis anterior, soleus, and gastocnemius during the stance phase of gait. Gait and Posture 2011; 34(1): 29-35.

[50] Wang R, Thur C, Gutierrez-Farewik E, Wretenberg P, Broström E. One year follow-up after operative ankle fractures: A prospective gait analysis study with a multi-segment foot model. Gait and Posture 2010; 31(2): 234-240.

[51] Buczek F, Rainbow M, Cooney K, Walker M, Sanders J. Implications of using hierarchical and six degree-of-freedom models for normal gait analyses. Gait and Posture 2010; 31(1): 57-63.

[52] Wolf S, Braatz F, Metaxiotis D, Armbrust P, Dreher T, Döderlein L, Mikut R. Gait analysis may help to distinguish hereditary spastic paraplegia from cerebral palsy. Gait and Posture 2011; 33(4): 556-561.

[53] Salazar-Torres J, McDowell B, Kerr C, Cosgrove A. Pelvic kinematics and their relationship to gait type in hemiplegic cerebral palsy. Gait and Posture 2011; 33(4): 620-624.

[54] Wren T, Otsuka N, Bowen R, Scaduto A, Chan L, Sheng M, Hara R, Kay R. Influence of gait analysis on decision-making for lower extremity orthopaedic surgery: Baseline data from a randomized controlled trial. Gait and Posture 2011; 34(3): 364-369.

[55] Tateuchi H, Tsukagoshi R, Fukumoto Y, Oda S. Immediate effects of different ankle pushoff instructions during walking exercise on hip kinematics and kinetics in individuals with total hip arthroplasty. Gait and Posture 2011; 33(4): 609-614.

[56] Stutzenberger G, Richter A, Schneider M, Mündermann A, Schwameder H. Effects of obesity on the biomechanics of stair-walking in children. Gait and Posture 2011; 34(1): 119-125.

[57] Bernhardt K, Oh T, Kaufman K. Gait patterns of patients with inclusion body myositis. Gait and Posture 2011; 33(3): 442-446.

[58] Cleophas T, Zwinderman A. Random effects models in clinical research. International Journal of Clinical Pharmacology Therapy 2008; 46(8): 421-427.

[59] DerSimonian R. Kacker R. Random-effects model for meta-analysis of clinical trials: An update. Contemporary Clinical Trials 2007; 28: 105-114.

[60] Hofmann M. Multi-view 3D human pose estimation combining single-frame recovery, temporal integration and model adaption. Computer Vision and Pattern Recognition 2009; IEEE conference on, On pages: 2214-2221.

[61] Lu T, O'Connor J. Bone position estimation from skin marker co-ordinates using global optimization with joint constraints. Journal of Biomechanics 1999; 32: 129-134.

[62] Kertis J, Fritz J, Long J, Harris GF. Static and Dynamic Calibration of an Eight-Camera Optical System for Human Motion Analysis. Critical Reviews in Physical and Rehabilitation Medicine 2010; 22(1): 49-59.

[63] Woltring H, A FORTRAN package for generalized, cross-validatory spline smoothing and differentiation. Advances in Engineering Software 1986; 8(2): 104-113.

[64] “Technology.” Technology. N.p., n.d. Web. 20 June 2012. <http://www.cyberneum.de/TrackingLab_en2.html>.

[65] “OptiTrack V100:R2 Actual Size Image.” Optitrack V100:R2 Actual Image Size. Web 20 June 2012. <http://pective.com/pic/optitrack-v100-r2>.

[66] “Motion Lab System Products.” Motion Lab Systems: Products: Quality Assurance: Knee Alignment Device. Web 20 June 2012. <http://emgsrus.com/prod_qa_kad.html>.

[67] “How to use Plug In Gait” Plug-In Gait. Web 20 June 2012. <www.irc-web.co.jp/vicon_web/news_bn/PIGManualver1.pdf>.

[68] “Anthropomorphic measures necessary for the Conventional Gait Model” Tutorial: Building a Conventional Gait Model. Web 7 August 2012. <http://www.c-motion.com/v3dwiki/index.php?title=Tutorial:_Building_a_Conventional_Gait_Model>.

[69] Stagni R, Leardini A, Cappozzo A, Benedetti M, Cappello A. Effects of hip joint centre mislocation on gait analysis results. Journal of Biomechanics 2000; 33: 1479-1487.

Appendix A

```
clear variables

ROOT = 'C:\Users\labadmin\Documents\c3d';
files = {
   '11_11_10_feet.c3d'
   '11_11_10_calf.c3d'
   '11_11_10_thigh.c3d'
   '11_11_10_hip.c3d'
   };
mkrnames = {
   'right_foot_R_Meta' 'RMETA'
   'right_foot_R_Heel' 'RHEEL'
   'right_foot_R_Ankle'    'RANKLE'
   'left_foot_L_Meta'  'LMETA'
   'left_foot_L_Heel'  'LHEEL'
   'left_foot_L_Ankle' 'LANKLE'
   'right_calf_R_knee' 'RKNEE'
   'right_calf_R_Ant_tib'    'RTIB'
   'left_calf_L_knee'    'LKNEE'
   'left_calf_L_ant_tib' 'LTIB'
   'right_thigh_R_ASIS' 'RASIS'
   'right_thigh_R_mid_thigh' 'RTHIGH'
   'left_thigh_L_ASIS' 'LASIS'
   'left_thigh_L_mid_thigh' 'LTHIGH'
   'Hip_PSIS' 'PSIS'
   };
c3d = c3dserver();

for i=1:numel(files);
   openc3d(c3d, 999, fullfile(ROOT, files{i}));
   if i == 1
      point(1).data = get3dtarget(c3d, mkrnames{1});
      point(2).data = get3dtarget(c3d, mkrnames{2});
      point(3).data = get3dtarget(c3d, mkrnames{3});
      point(4).data = get3dtarget(c3d, mkrnames{4});
      point(5).data = get3dtarget(c3d, mkrnames{5});
      point(6).data = get3dtarget(c3d, mkrnames{6});
      closec3d(c3d);
   end
   if i == 2
      point(7).data = get3dtarget(c3d, mkrnames{7});
      point(8).data = get3dtarget(c3d, mkrnames{8});
      point(9).data = get3dtarget(c3d, mkrnames{9});
      point(10).data = get3dtarget(c3d, mkrnames{10});
      closec3d(c3d);
   end
   if i == 3
      point(11).data = get3dtarget(c3d, mkrnames{11});
      point(12).data = get3dtarget(c3d, mkrnames{12});
      point(13).data = get3dtarget(c3d, mkrnames{13});
      point(14).data = get3dtarget(c3d, mkrnames{14});
      closec3d(c3d);
```

```
    end

    if i == 4
        point(15).data = get3dtarget(c3d, mkrnames{15});
        closec3d(c3d);
    end

end

c3d2 = c3dserver();
createc3d(c3d2,'composite_data',100,size(point(1).data,1),0,13,0,1,2,0.1)
for i = 1:numel(point)
    fprintf(['Processing ', mkrnames{i,1}, '...\n']);
    inds_nan = find(isnan(point(i).data(:,1)));
    if not(isempty(inds_nan))
        point(i).data(inds_nan,:) = zeros(numel(inds_nan),3);
    end
    c3d2 = add_marker_data(c3d2, mkrnames{i,2}, point(i).data);
end
newfilename = fullfile(ROOT,'jeff_new_c3d.c3d');
savec3d(c3d2,newfilename,-1)
```

Appendix B

```
clc
close all
clear all

Hip_flexion_extension = xlsread('edited_dynamic_subject_K9.csv','BG53:BG159');
Hip_ab_adduction = xlsread('edited_dynamic_subject_K9.csv','BH53:BH159');
Hip_rotation = xlsread('edited_dynamic_subject_K9.csv','BI53:BI159');
Knee_flexion_extension = xlsread('edited_dynamic_subject_K9.csv','BJ53:BJ159');
Knee_varus_valgus = xlsread('edited_dynamic_subject_K9.csv','BK53:BK159');
Tibial_rotation = xlsread('edited_dynamic_subject_K9.csv','BL53:BL159');
Ankle_flexion_extension = xlsread('edited_dynamic_subject_K9.csv','BM53:BM159');
Foot_progression = xlsread('edited_dynamic_subject_K9.csv','CD53:CD159');
Ankle_rotation = xlsread('edited_dynamic_subject_K9.csv','BO53:BO159');
Pelvic_tilt = xlsread('edited_dynamic_subject_K9.csv','BV53:BV159');
Pelvic_obliquity = xlsread('edited_dynamic_subject_K9.csv','BW53:BW159');
Pelvic_rotation = xlsread('edited_dynamic_subject_K9.csv','BX53:BX159');

data_range_value = (length(Hip_flexion_extension));

original_time = linspace(0,100,data_range_value)';

percent_gait_cycle_time = linspace(0,100,100)';

A = interp1(original_time,Hip_flexion_extension,percent_gait_cycle_time);
B = interp1(original_time,Hip_ab_adduction,percent_gait_cycle_time);
C = interp1(original_time,Hip_rotation,percent_gait_cycle_time);
D = interp1(original_time,Knee_flexion_extension,percent_gait_cycle_time);
E = interp1(original_time,Knee_varus_valgus,percent_gait_cycle_time);
F = interp1(original_time,Tibial_rotation,percent_gait_cycle_time);
G = interp1(original_time,Ankle_flexion_extension,percent_gait_cycle_time);
H = interp1(original_time,Foot_progression,percent_gait_cycle_time);
I = interp1(original_time,Ankle_rotation,percent_gait_cycle_time);
J = interp1(original_time,Pelvic_tilt,percent_gait_cycle_time);
K = interp1(original_time,Pelvic_obliquity,percent_gait_cycle_time);
L = interp1(original_time,Pelvic_rotation,percent_gait_cycle_time);

Adjusted_data = [A B C D E F G H I J K L];

xlswrite('convert_gait_cycle_K9.xls', Adjusted_data)
```

Appendix C

```
clear all
clc

X = Sagittal Plane
Y = Coronal Plane
Z = Transverse Plane

Right Side summation of trial data

A1 = xlsread('convert_gait_cycle_A1.xls');
A2 = xlsread('convert_gait_cycle_A2.xls');
A3 = xlsread('convert_gait_cycle_A3.xls');
B1 = xlsread('convert_gait_cycle_B1.xls');
B2 = xlsread('convert_gait_cycle_B2.xls');
B4 = xlsread('convert_gait_cycle_B4.xls');
C1 = xlsread('convert_gait_cycle_C1.xls');
C3 = xlsread('convert_gait_cycle_C3.xls');
C5 = xlsread('convert_gait_cycle_C5.xls');
E1 = xlsread('convert_gait_cycle_E1.xls');
E6 = xlsread('convert_gait_cycle_E6.xls');
E7 = xlsread('convert_gait_cycle_E7.xls');
F1 = xlsread('convert_gait_cycle_F1.xls');
F2 = xlsread('convert_gait_cycle_F2.xls');
F4 = xlsread('convert_gait_cycle_F4.xls');
G1 = xlsread('convert_gait_cycle_G1.xls');
G2 = xlsread('convert_gait_cycle_G2.xls');
G3 = xlsread('convert_gait_cycle_G3.xls');
H1 = xlsread('convert_gait_cycle_H1.xls');
H2 = xlsread('convert_gait_cycle_H2.xls');
H4 = xlsread('convert_gait_cycle_H4.xls');
I2 = xlsread('convert_gait_cycle_I2.xls');
I3 = xlsread('convert_gait_cycle_I3.xls');
I4 = xlsread('convert_gait_cycle_I4.xls');
J3 = xlsread('convert_gait_cycle_J3.xls');
J4 = xlsread('convert_gait_cycle_J4.xls');
J5 = xlsread('convert_gait_cycle_J5.xls');
K7 = xlsread('convert_gait_cycle_K7.xls');
K8 = xlsread('convert_gait_cycle_K8.xls');
K9 = xlsread('convert_gait_cycle_K9.xls');

pelvis_right_x = [A1(:,10) A2(:,10) A3(:,10) B1(:,10) B2(:,10) B4(:,10)...
   C1(:,10) C3(:,10) C5(:,10) E1(:,10) E6(:,10) E7(:,10) F1(:,10) F2(:,10)...
   F4(:,10) G1(:,10) G2(:,10) G3(:,10) H1(:,10) H2(:,10) H4(:,10) I2(:,10)...
   I3(:,10) I4(:,10) J3(:,10) J4(:,10) J5(:,10) K7(:,10) K8(:,10) K9(:,10)];

pelvis_right_y = [A1(:,11) A2(:,11) A3(:,11) B1(:,11) B2(:,11) B4(:,11)...
   C1(:,11) C3(:,11) C5(:,11) E1(:,11) E6(:,11) E7(:,11) F1(:,11) F2(:,11)...
   F4(:,11) G1(:,11) G2(:,11) G3(:,11) H1(:,11) H2(:,11) H4(:,11) I2(:,11)...
   I3(:,11) I4(:,11) J3(:,11) J4(:,11) J5(:,11) K7(:,11) K8(:,11) K9(:,11)];

pelvis_right_z = [A1(:,12) A2(:,12) A3(:,12) B1(:,12) B2(:,12) B4(:,12)...
```

```
    C1(:,12) C3(:,12) C5(:,12) E1(:,12) E6(:,12) E7(:,12) F1(:,12) F2(:,12)...
    F4(:,12) G1(:,12) G2(:,12) G3(:,12) H1(:,12) H2(:,12) H4(:,12) I2(:,12)...
    I3(:,12) I4(:,12) J3(:,12) J4(:,12) J5(:,12) K7(:,12) K8(:,12) K9(:,12)];

hip_right_x = [A1(:,1) A2(:,1) A3(:,1) B1(:,1) B2(:,1) B4(:,1)...
    C1(:,1) C3(:,1) C5(:,1) E1(:,1) E6(:,1) E7(:,1) F1(:,1) F2(:,1)...
    F4(:,1) G1(:,1) G2(:,1) G3(:,1) H1(:,1) H2(:,1) H4(:,1) I2(:,1)...
    I3(:,1) I4(:,1) J3(:,1) J4(:,1) J5(:,1) K7(:,1) K8(:,1) K9(:,1)];

hip_right_y = [A1(:,2) A2(:,2) A3(:,2) B1(:,2) B2(:,2) B4(:,2)...
    C1(:,2) C3(:,2) C5(:,2) E1(:,2) E6(:,2) E7(:,2) F1(:,2) F2(:,2)...
    F4(:,2) G1(:,2) G2(:,2) G3(:,2) H1(:,2) H2(:,2) H4(:,2) I2(:,2)...
    I3(:,2) I4(:,2) J3(:,2) J4(:,2) J5(:,2) K7(:,2) K8(:,2) K9(:,2)];

hip_right_z = [A1(:,3) A2(:,3) A3(:,3) B1(:,3) B2(:,3) B4(:,3)...
    C1(:,3) C3(:,3) C5(:,3) E1(:,3) E6(:,3) E7(:,3) F1(:,3) F2(:,3)...
    F4(:,3) G1(:,3) G2(:,3) G3(:,3) H1(:,3) H2(:,3) H4(:,3) I2(:,3)...
    I3(:,3) I4(:,3) J3(:,3) J4(:,3) J5(:,3) K7(:,3) K8(:,3) K9(:,3)];

knee_right_x = [A1(:,4) A2(:,4) A3(:,4) B1(:,4) B2(:,4) B4(:,4)...
    C1(:,4) C3(:,4) C5(:,4) E1(:,4) E6(:,4) E7(:,4) F1(:,4) F2(:,4)...
    F4(:,4) G1(:,4) G2(:,4) G3(:,4) H1(:,4) H2(:,4) H4(:,4) I2(:,4)...
    I3(:,4) I4(:,4) J3(:,4) J4(:,4) J5(:,4) K7(:,4) K8(:,4) K9(:,4)];

knee_right_y = [A1(:,5) A2(:,5) A3(:,5) B1(:,5) B2(:,5) B4(:,5)...
    C1(:,5) C3(:,5) C5(:,5) E1(:,5) E6(:,5) E7(:,5) F1(:,5) F2(:,5)...
    F4(:,5) G1(:,5) G2(:,5) G3(:,5) H1(:,5) H2(:,5) H4(:,5) I2(:,5)...
    I3(:,5) I4(:,5) J3(:,5) J4(:,5) J5(:,5) K7(:,5) K8(:,5) K9(:,5)];

knee_right_z = [A1(:,6) A2(:,6) A3(:,6) B1(:,6) B2(:,6) B4(:,6)...
    C1(:,6) C3(:,6) C5(:,6) E1(:,6) E6(:,6) E7(:,6) F1(:,6) F2(:,6)...
    F4(:,6) G1(:,6) G2(:,6) G3(:,6) H1(:,6) H2(:,6) H4(:,6) I2(:,6)...
    I3(:,6) I4(:,6) J3(:,6) J4(:,6) J5(:,6) K7(:,6) K8(:,6) K9(:,6)];

ankle_right_x = [A1(:,7) A2(:,7) A3(:,7) B1(:,7) B2(:,7) B4(:,7)...
    C1(:,7) C3(:,7) C5(:,7) E1(:,7) E6(:,7) E7(:,7) F1(:,7) F2(:,7)...
    F4(:,7) G1(:,7) G2(:,7) G3(:,7) H1(:,7) H2(:,7) H4(:,7) I2(:,7)...
    I3(:,7) I4(:,7) J3(:,7) J4(:,7) J5(:,7) K7(:,7) K8(:,7) K9(:,7)];

ankle_right_y = [A1(:,8) A2(:,8) A3(:,8) B1(:,8) B2(:,8) B4(:,8)...
    C1(:,8) C3(:,8) C5(:,8) E1(:,8) E6(:,8) E7(:,8) F1(:,8) F2(:,8)...
    F4(:,8) G1(:,8) G2(:,8) G3(:,8) H1(:,8) H2(:,8) H4(:,8) I2(:,8)...
    I3(:,8) I4(:,8) J3(:,8) J4(:,8) J5(:,8) K7(:,8) K8(:,8) K9(:,8)];

ankle_right_z = [A1(:,9) A2(:,9) A3(:,9) B1(:,9) B2(:,9) B4(:,9)...
    C1(:,9) C3(:,9) C5(:,9) E1(:,9) E6(:,9) E7(:,9) F1(:,9) F2(:,9)...
    F4(:,9) G1(:,9) G2(:,9) G3(:,9) H1(:,9) H2(:,9) H4(:,9) I2(:,9)...
    I3(:,9) I4(:,9) J3(:,9) J4(:,9) J5(:,9) K7(:,9) K8(:,9) K9(:,9)];

xlswrite('Right_side_vicon_data.xls',pelvis_right_x,'pelvis_right_x')
xlswrite('Right_side_vicon_data.xls',pelvis_right_y,'pelvis_right_y')
xlswrite('Right_side_vicon_data.xls',pelvis_right_z,'pelvis_right_z')
xlswrite('Right_side_vicon_data.xls',hip_right_x,'hip_right_x')
xlswrite('Right_side_vicon_data.xls',hip_right_y,'hip_right_y')
```

```
xlswrite('Right_side_vicon_data.xls',hip_right_z,'hip_right_z')
xlswrite('Right_side_vicon_data.xls',knee_right_x,'knee_right_x')
xlswrite('Right_side_vicon_data.xls',knee_right_y,'knee_right_y')
xlswrite('Right_side_vicon_data.xls',knee_right_z,'knee_right_z')
xlswrite('Right_side_vicon_data.xls',ankle_right_x,'ankle_right_x')
xlswrite('Right_side_vicon_data.xls',ankle_right_y,'ankle_right_y')
xlswrite('Right_side_vicon_data.xls',ankle_right_z,'ankle_right_z')

% Left Side summation of trial data

A7 = xlsread('convert_gait_cycle_A7.xls');
A8 = xlsread('convert_gait_cycle_A8.xls');
A10 = xlsread('convert_gait_cycle_A10.xls');
B9 = xlsread('convert_gait_cycle_B9.xls');
B10 = xlsread('convert_gait_cycle_B10.xls');
B11= xlsread('convert_gait_cycle_B11.xls');
C2 = xlsread('convert_gait_cycle_C2.xls');
C9 = xlsread('convert_gait_cycle_C9.xls');
C10 = xlsread('convert_gait_cycle_C10.xls');
E8 = xlsread('convert_gait_cycle_E8.xls');
E9 = xlsread('convert_gait_cycle_E9.xls');
E11 = xlsread('convert_gait_cycle_E11.xls');
F7 = xlsread('convert_gait_cycle_F7.xls');
F8 = xlsread('convert_gait_cycle_F8.xls');
F10 = xlsread('convert_gait_cycle_F10.xls');
G7 = xlsread('convert_gait_cycle_G7.xls');
G8 = xlsread('convert_gait_cycle_G8.xls');
G9 = xlsread('convert_gait_cycle_G9.xls');
H7 = xlsread('convert_gait_cycle_H7.xls');
H10 = xlsread('convert_gait_cycle_H10.xls');
H11 = xlsread('convert_gait_cycle_H11.xls');
I7 = xlsread('convert_gait_cycle_I7.xls');
I8 = xlsread('convert_gait_cycle_I8.xls');
I9 = xlsread('convert_gait_cycle_I9.xls');
J8 = xlsread('convert_gait_cycle_J8.xls');
J9 = xlsread('convert_gait_cycle_J9.xls');
J11 = xlsread('convert_gait_cycle_J11.xls');
K4 = xlsread('convert_gait_cycle_K4.xls');
K5 = xlsread('convert_gait_cycle_K5.xls');
K6 = xlsread('convert_gait_cycle_K6.xls');

pelvis_left_x = [A7(:,10) A8(:,10) A10(:,10) B9(:,10) B10(:,10) B11(:,10)...
    C2(:,10) C9(:,10) C10(:,10) E8(:,10) E9(:,10) E11(:,10) F7(:,10) F8(:,10)...
    F10(:,10) G7(:,10) G8(:,10) G9(:,10) H7(:,10) H10(:,10) H11(:,10) I7(:,10)...
    I8(:,10) I9(:,10) J8(:,10) J9(:,10) J11(:,10) K4(:,10) K5(:,10) K6(:,10)];

pelvis_left_y = [A7(:,11) A8(:,11) A10(:,11) B9(:,11) B10(:,11) B11(:,11)...
    C2(:,11) C9(:,11) C10(:,11) E8(:,11) E9(:,11) E11(:,11) F7(:,11) F8(:,11)...
    F10(:,11) G7(:,11) G8(:,11) G9(:,11) H7(:,11) H10(:,11) H11(:,11) I7(:,11)...
    I8(:,11) I9(:,11) J8(:,11) J9(:,11) J11(:,11) K4(:,11) K5(:,11) K6(:,11)];

pelvis_left_z = [A7(:,12) A8(:,12) A10(:,12) B9(:,12) B10(:,12) B11(:,12)...
    C2(:,12) C9(:,12) C10(:,12) E8(:,12) E9(:,12) E11(:,12) F7(:,12) F8(:,12)...
    F10(:,12) G7(:,12) G8(:,12) G9(:,12) H7(:,12) H10(:,12) H11(:,12) I7(:,12)...
    I8(:,12) I9(:,12) J8(:,12) J9(:,12) J11(:,12) K4(:,12) K5(:,12) K6(:,12)];
```

```
hip_left_x = [A7(:,1) A8(:,1) A10(:,1) B9(:,1) B10(:,1) B11(:,1)...
    C2(:,1) C9(:,1) C10(:,1) E8(:,1) E9(:,1) E11(:,1) F7(:,1) F8(:,1)...
    F10(:,1) G7(:,1) G8(:,1) G9(:,1) H7(:,1) H10(:,1) H11(:,1) I7(:,1)...
    I8(:,1) I9(:,1) J8(:,1) J9(:,1) J11(:,1) K4(:,1) K5(:,1) K6(:,1)];

hip_left_y = [A7(:,2) A8(:,2) A10(:,2) B9(:,2) B10(:,2) B11(:,2)...
    C2(:,2) C9(:,2) C10(:,2) E8(:,2) E9(:,2) E11(:,2) F7(:,2) F8(:,2)...
    F10(:,2) G7(:,2) G8(:,2) G9(:,2) H7(:,2) H10(:,2) H11(:,2) I7(:,2)...
    I8(:,2) I9(:,2) J8(:,2) J9(:,2) J11(:,2) K4(:,2) K5(:,2) K6(:,2)];

hip_left_z = [A7(:,3) A8(:,3) A10(:,3) B9(:,3) B10(:,3) B11(:,3)...
    C2(:,3) C9(:,3) C10(:,3) E8(:,3) E9(:,3) E11(:,3) F7(:,3) F8(:,3)...
    F10(:,3) G7(:,3) G8(:,3) G9(:,3) H7(:,3) H10(:,3) H11(:,3) I7(:,3)...
    I8(:,3) I9(:,3) J8(:,3) J9(:,3) J11(:,3) K4(:,3) K5(:,3) K6(:,3)];

knee_left_x = [A7(:,4) A8(:,4) A10(:,4) B9(:,4) B10(:,4) B11(:,4)...
    C2(:,4) C9(:,4) C10(:,4) E8(:,4) E9(:,4) E11(:,4) F7(:,4) F8(:,4)...
    F10(:,4) G7(:,4) G8(:,4) G9(:,4) H7(:,4) H10(:,4) H11(:,4) I7(:,4)...
    I8(:,4) I9(:,4) J8(:,4) J9(:,4) J11(:,4) K4(:,4) K5(:,4) K6(:,4)];

knee_left_y = [A7(:,5) A8(:,5) A10(:,5) B9(:,5) B10(:,5) B11(:,5)...
    C2(:,5) C9(:,5) C10(:,5) E8(:,5) E9(:,5) E11(:,5) F7(:,5) F8(:,5)...
    F10(:,5) G7(:,5) G8(:,5) G9(:,5) H7(:,5) H10(:,5) H11(:,5) I7(:,5)...
    I8(:,5) I9(:,5) J8(:,5) J9(:,5) J11(:,5) K4(:,5) K5(:,5) K6(:,5)];

knee_left_z = [A7(:,6) A8(:,6) A10(:,6) B9(:,6) B10(:,6) B11(:,6)...
    C2(:,6) C9(:,6) C10(:,6) E8(:,6) E9(:,6) E11(:,6) F7(:,6) F8(:,6)...
    F10(:,6) G7(:,6) G8(:,6) G9(:,6) H7(:,6) H10(:,6) H11(:,6) I7(:,6)...
    I8(:,6) I9(:,6) J8(:,6) J9(:,6) J11(:,6) K4(:,6) K5(:,6) K6(:,6)];

ankle_left_x = [A7(:,7) A8(:,7) A10(:,7) B9(:,7) B10(:,7) B11(:,7)...
    C2(:,7) C9(:,7) C10(:,7) E8(:,7) E9(:,7) E11(:,7) F7(:,7) F8(:,7)...
    F10(:,7) G7(:,7) G8(:,7) G9(:,7) H7(:,7) H10(:,7) H11(:,7) I7(:,7)...
    I8(:,7) I9(:,7) J8(:,7) J9(:,7) J11(:,7) K4(:,7) K5(:,7) K6(:,7)];

ankle_left_y = [A7(:,8) A8(:,8) A10(:,8) B9(:,8) B10(:,8) B11(:,8)...
    C2(:,8) C9(:,8) C10(:,8) E8(:,8) E9(:,8) E11(:,8) F7(:,8) F8(:,8)...
    F10(:,8) G7(:,8) G8(:,8) G9(:,8) H7(:,8) H10(:,8) H11(:,8) I7(:,8)...
    I8(:,8) I9(:,8) J8(:,8) J9(:,8) J11(:,8) K4(:,8) K5(:,8) K6(:,8)];

ankle_left_z = [A7(:,9) A8(:,9) A10(:,9) B9(:,9) B10(:,9) B11(:,9)...
    C2(:,9) C9(:,9) C10(:,9) E8(:,9) E9(:,9) E11(:,9) F7(:,9) F8(:,9)...
    F10(:,9) G7(:,9) G8(:,9) G9(:,9) H7(:,9) H10(:,9) H11(:,9) I7(:,9)...
    I8(:,9) I9(:,9) J8(:,9) J9(:,9) J11(:,9) K4(:,9) K5(:,9) K6(:,9)];

xlswrite('left_side_vicon_data.xls',pelvis_left_x,'pelvis_left_x')
xlswrite('left_side_vicon_data.xls',pelvis_left_y,'pelvis_left_y')
xlswrite('left_side_vicon_data.xls',pelvis_left_z,'pelvis_left_z')
xlswrite('left_side_vicon_data.xls',hip_left_x,'hip_left_x')
xlswrite('left_side_vicon_data.xls',hip_left_y,'hip_left_y')
xlswrite('left_side_vicon_data.xls',hip_left_z,'hip_left_z')
xlswrite('left_side_vicon_data.xls',knee_left_x,'knee_left_x')
xlswrite('left_side_vicon_data.xls',knee_left_y,'knee_left_y')
```

```
xlswrite('left_side_vicon_data.xls',knee_left_z,'knee_left_z')
xlswrite('left_side_vicon_data.xls',ankle_left_x,'ankle_left_x')
xlswrite('left_side_vicon_data.xls',ankle_left_y,'ankle_left_y')
xlswrite('left_side_vicon_data.xls',ankle_left_z,'ankle_left_z')
```

Appendix D

Figure 16: Image of L-frame.

Figure 17: Image of calibration wand.

Figure 18: Image of camera set up.

Figure 19: Additional image of camera set up on same side.

Figure 20: Image of camera set up for opposite side.

Figure 21: Image of entire capture volume.

Appendix E

Table 10: Temporal and Stride parameters of each subject and averages for the right side with Visual3D.

Right - Temporal and Stride Parameters (Visual3D)				
Subject	Cadence (steps/min)	Walk Speed (m/s)	Step Length (m)	Stride Length (m)
A	117.463	1.239	0.671	1.293
B	114.795	1.242	0.633	1.277
C	106.246	1.110	0.609	1.241
E	115.315	1.166	0.590	1.209
F	107.299	1.171	0.645	1.289
G	105.976	1.244	0.691	1.420
H	116.628	1.301	0.662	1.149
I	102.864	1.054	0.585	1.225
J	105.285	1.075	0.619	1.254
K	108.488	1.063	0.577	1.141
Average (Male)	108.015	1.135	0.629	1.267
Average (Female)	112.057	1.198	0.628	1.233
Average Overall	110.036	1.167	0.628	1.250

Table 11: Temporal and Stride parameters of each subject and averages for the left side with Visual3D.

Left -Temporal and Stride Parameters (Visual3D)				
Subject	Cadence (steps/min)	Walk Speed (m/s)	Step Length (m)	Stride Length (m)
A	122.108	1.356	0.645	1.322
B	120.080	1.241	0.629	1.254
C	111.137	1.162	0.621	1.259
E	118.228	1.231	0.637	1.251
F	109.764	1.226	0.655	1.320
G	102.319	1.191	0.682	1.369
H	118.462	1.319	0.670	1.356
I	104.680	1.105	0.650	1.286
J	101.244	1.089	0.649	1.295
K	116.167	1.057	0.528	1.099
Average (Male)	109.304	1.160	0.631	1.274
Average (Female)	115.534	1.236	0.642	1.288
Average Overall	112.419	1.198	0.637	1.281

Table 12: Temporal and Stride parameters of each subject and averages for the right side with Nexus.

Right -Temporal and Stride Parameters (Nexus)				
Subject	Cadence (steps/min)	Walk Speed (m/s)	Step Length (m)	Stride Length (m)
A	116.146	1.248	0.659	1.290
B	116.657	1.238	0.617	1.273
C	107.080	1.112	0.606	1.245
E	115.857	1.168	0.577	1.208
F	109.508	1.176	0.633	1.287
G	104.726	1.242	0.693	1.423
H	115.786	1.285	0.654	1.332
I	101.468	1.046	0.589	1.236
J	101.985	1.069	0.617	1.258
K	112.156	1.063	0.556	1.138
Average (Male)	107.296	1.134	0.623	1.269
Average (Female)	112.978	1.196	0.617	1.269
Average Overall	110.137	1.165	0.620	1.269

Table 13: Temporal and Stride parameters of each subject and averages for the left side with Nexus.

Left - Temporal and Stride Parameters (Nexus)				
Subject	Cadence (steps/min)	Walk Speed (m/s)	Step Length (m)	Stride Length (m)
A	123.361	1.345	0.636	1.308
B	119.224	1.247	0.641	1.256
C	111.130	1.161	0.617	1.254
E	117.715	1.219	0.628	1.242
F	111.830	1.230	0.662	1.320
G	105.263	1.197	0.677	1.364
H	118.051	1.335	0.680	1.357
I	103.759	1.109	0.643	1.282
J	101.410	1.095	0.638	1.296
K	116.175	1.068	0.550	1.103
Average (Male)	109.994	1.163	0.629	1.271
Average (Female)	115.590	1.239	0.646	1.286
Average Overall	112.792	1.201	0.637	1.278

Appendix F

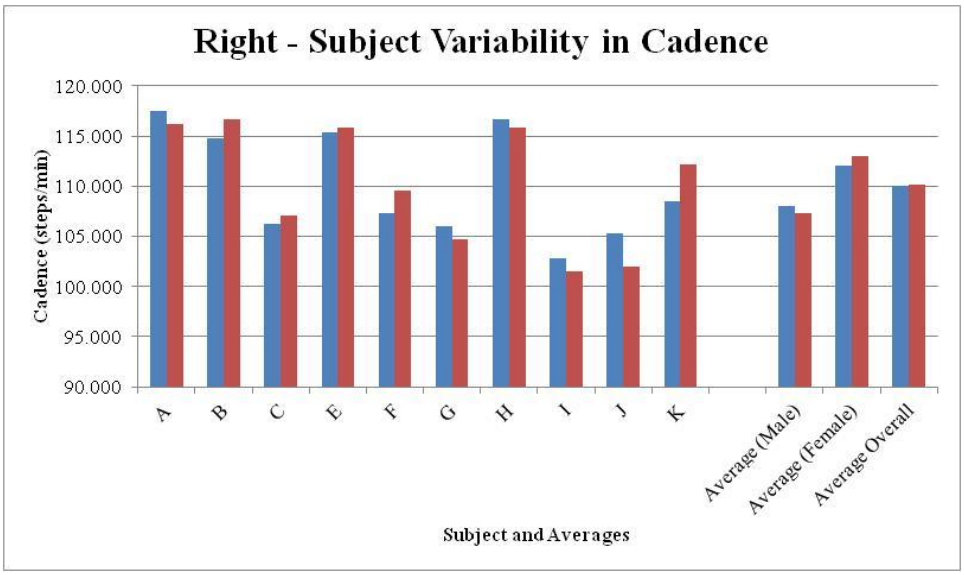

Figure 22: Variability of subject cadence and averages for the right side between Nexus and Visual3D. Blue is Visual3D and red is Nexus.

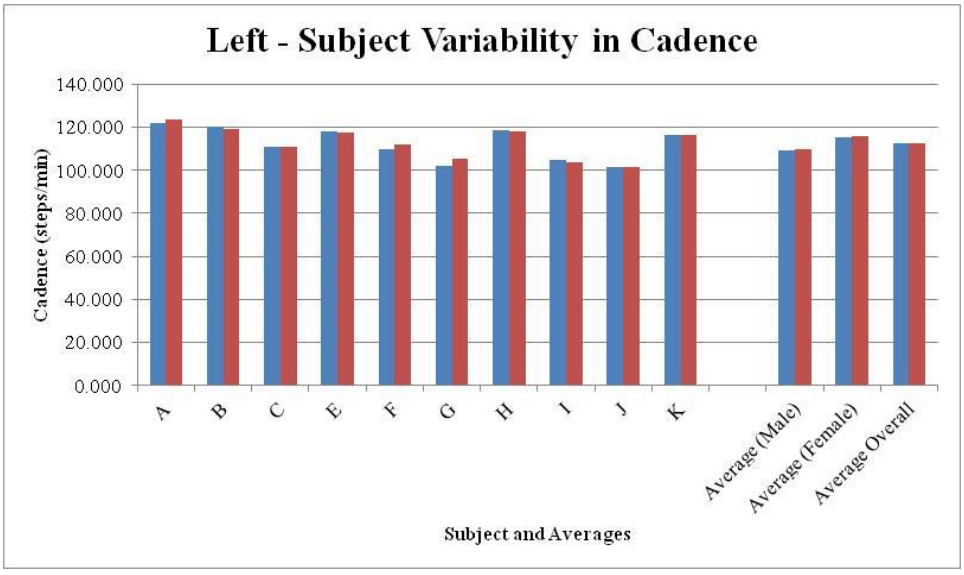

Figure 23: Variability of subject cadence and averages for the left side between Nexus and Visual3D. Blue is Visual3D and red is Nexus.

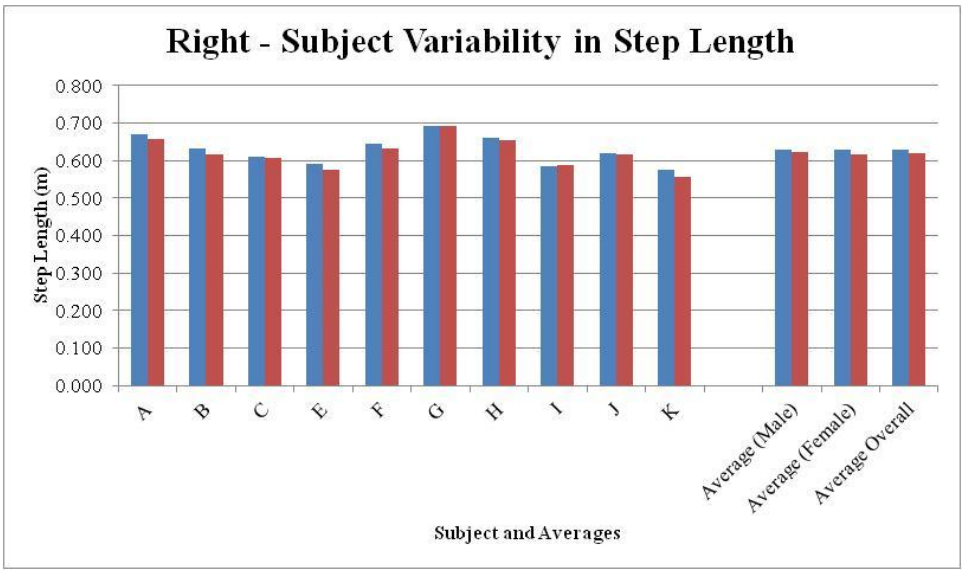

Figure 24: Variability of subject step length and averages for the right side between Nexus and Visual3D. Blue is Visual3D and red is Nexus.

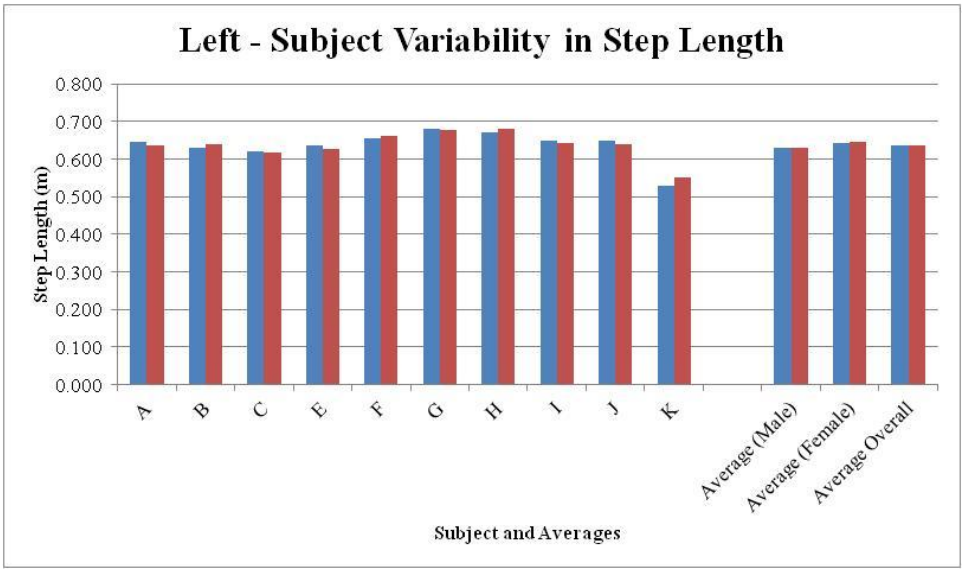

Figure 25: Variability of subject step length and averages for the left side between Nexus and Visual3D. Blue is Visual3D and red is Nexus.

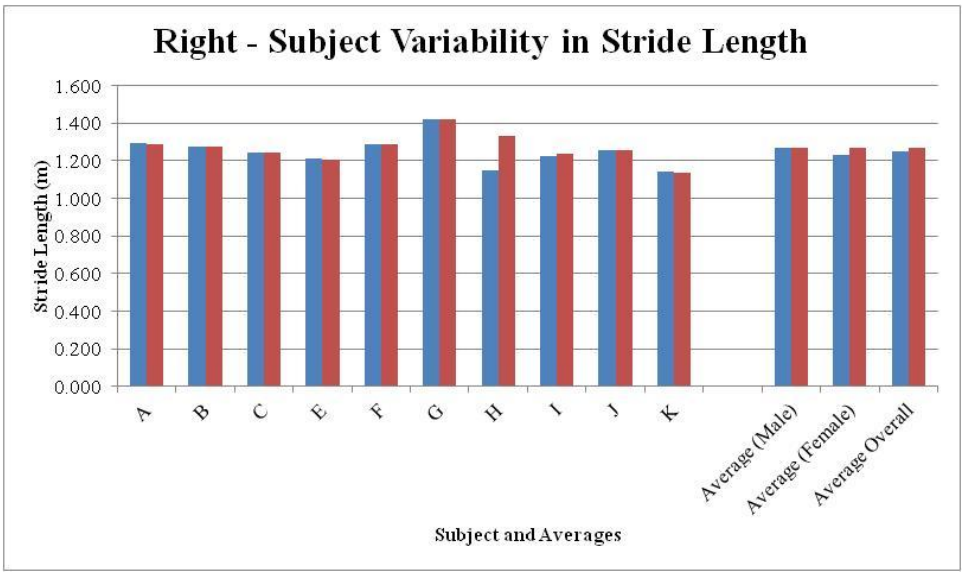

Figure 26: Variability of subject stride length and averages for the right side between Nexus and Visual3D. Blue is Visual3D and red is Nexus.

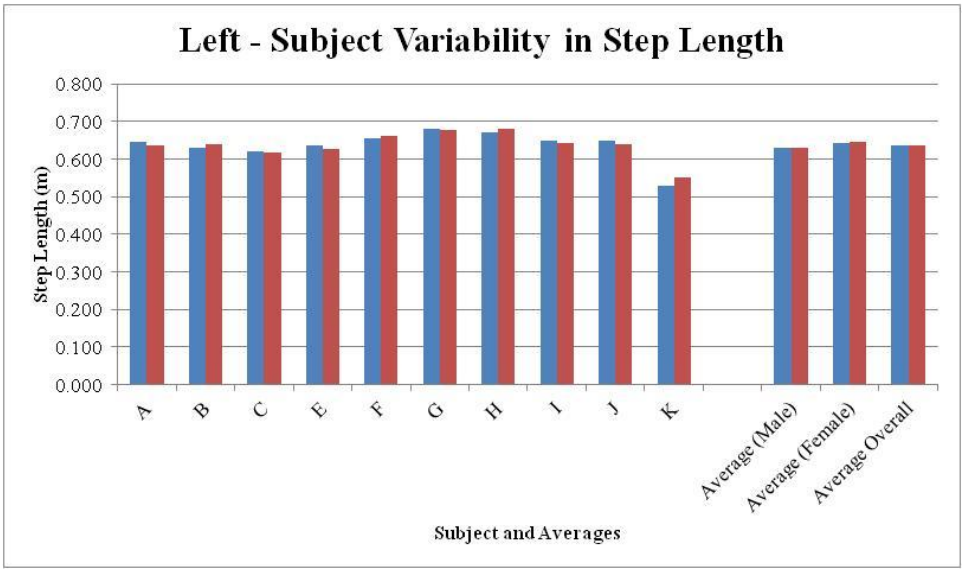

Figure 27: Variability of subject stride length and averages for the left side between Nexus and Visual3D. Blue is Visual3D and red is Nexus.

Table 14: Maximum, minimum, and range values for Visual3D, Nexus, and control Study.

	Max			Min			Difference		
	Visual3D	Nexus	Control	Visual3D	Nexus	Control	Visual3D	Nexus	Control
Left Pelvic Tilt	7.79	7.86	8.35	5.84	5.86	6.87	1.94	2.00	1.48
Left Pelvic Obliquity	5.25	5.20	4.41	-5.08	-5.02	-4.28	10.34	10.22	8.69
LeftPelvic Rotation	7.32	5.69	3.76	-4.02	-3.04	-3.62	11.35	8.74	7.38
Left Hip Flexion/Extension	30.23	28.85	28.77	-11.74	-13.07	-12.09	41.96	41.92	40.86
Left Hip Ab/Adduction	5.81	5.79	3.30	-9.13	-9.65	-9.82	14.94	15.44	13.12
Left Hip Rotation	3.00	5.56	8.16	-8.84	-7.82	-2.09	11.84	13.38	10.24
Left Knee Flexion/Extension	62.39	62.32	60.22	3.85	2.92	2.46	58.54	59.40	57.77
Left Knee Valgus/Varus	6.82	8.22	13.16	1.61	2.41	4.28	5.21	5.81	8.88
Left Tibial Rotation	13.37	11.25	6.57	-1.69	-2.51	-4.77	15.05	13.76	11.33
Left Foot Dorsi Plantar	13.85	14.99	13.76	-11.64	-15.41	-11.30	25.49	30.40	25.06
Left Foot Progression	-2.74	-0.66	-3.17	-11.48	-9.88	-14.19	8.75	9.22	11.02
Left Foot Rotation	-6.22	-0.57	-3.93	-18.55	-16.55	-14.82	12.33	15.97	10.89
Right Pelvic Tilt	7.65	7.71	8.35	5.25	5.23	6.87	2.40	2.48	1.48
Right Pelvic Obliquity	4.74	4.70	4.41	-4.98	-4.95	-4.28	9.71	9.64	8.69
RightPelvic Rotation	3.57	2.89	3.76	-6.42	-4.99	-3.62	10.00	7.88	7.38
Right Hip Flexion/Extension	29.49	28.34	28.77	-11.26	-12.84	-12.09	40.75	41.18	40.86
Right Hip Ab/Adduction	6.64	6.60	3.30	-7.84	-8.23	-9.82	14.48	14.83	13.12
Right Hip Rotation	4.77	6.81	8.16	-4.88	-5.01	-2.09	9.66	11.81	10.24
Right Knee Flexion/Extension	61.44	61.91	60.22	3.44	3.03	2.46	58.01	58.88	57.77
Right Knee Valgus/Varus	6.82	8.02	13.16	1.44	1.72	4.28	5.38	6.30	8.88
Right Tibial Rotation	18.13	14.56	6.57	0.27	-1.15	-4.77	17.86	15.71	11.33
Right Foot Dorsi Plantar	14.92	15.30	13.76	-8.78	-12.90	-11.30	23.71	28.21	25.06
Right Foot Progression	-5.16	-1.72	-3.17	-13.51	-11.43	-14.19	8.36	9.72	11.02
Right Foot Rotation	-11.31	-6.08	-3.93	-24.78	-18.69	-14.82	13.47	12.61	10.89

Appendix H

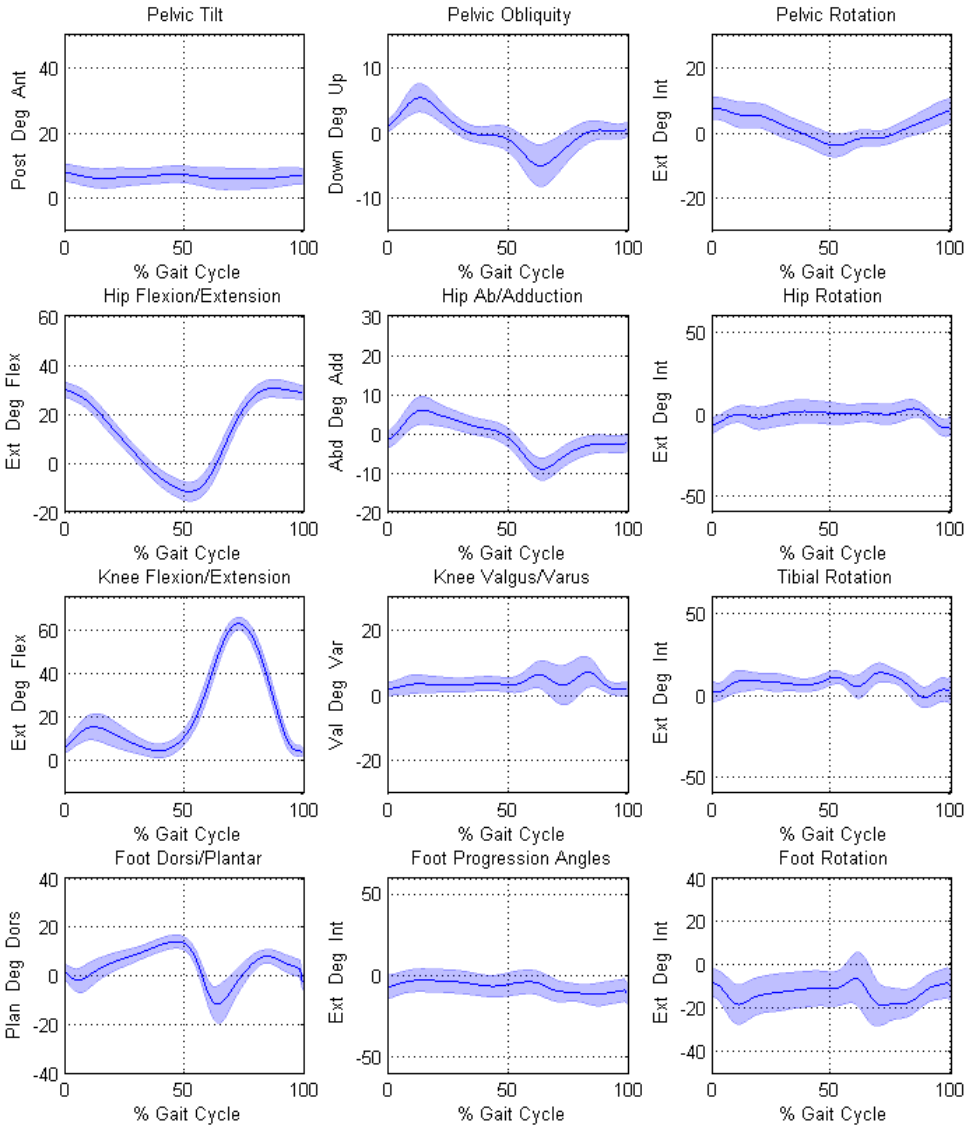

Figure 28: Visual3D plots of joint angle data for the left side.

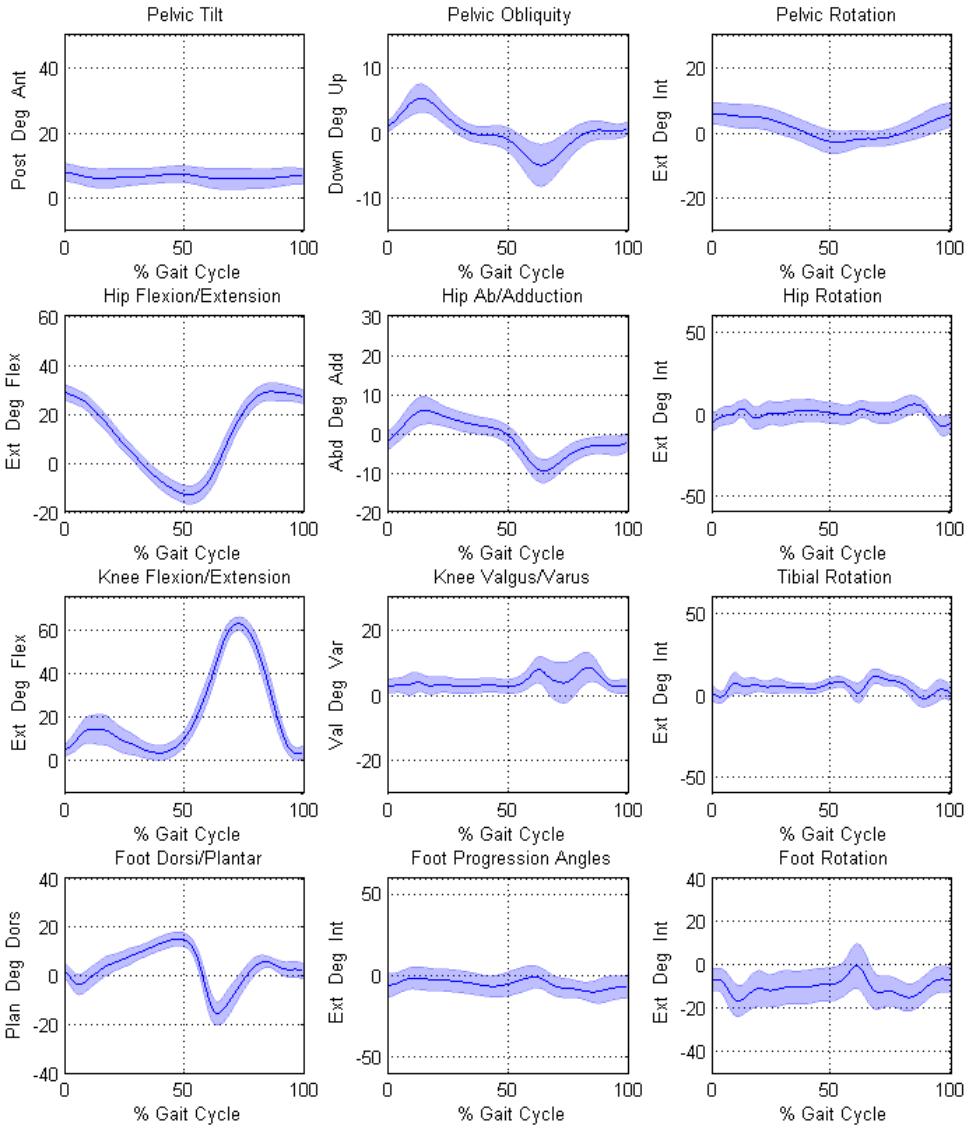

Figure 29: Nexus plots of joint angle data for the left side.

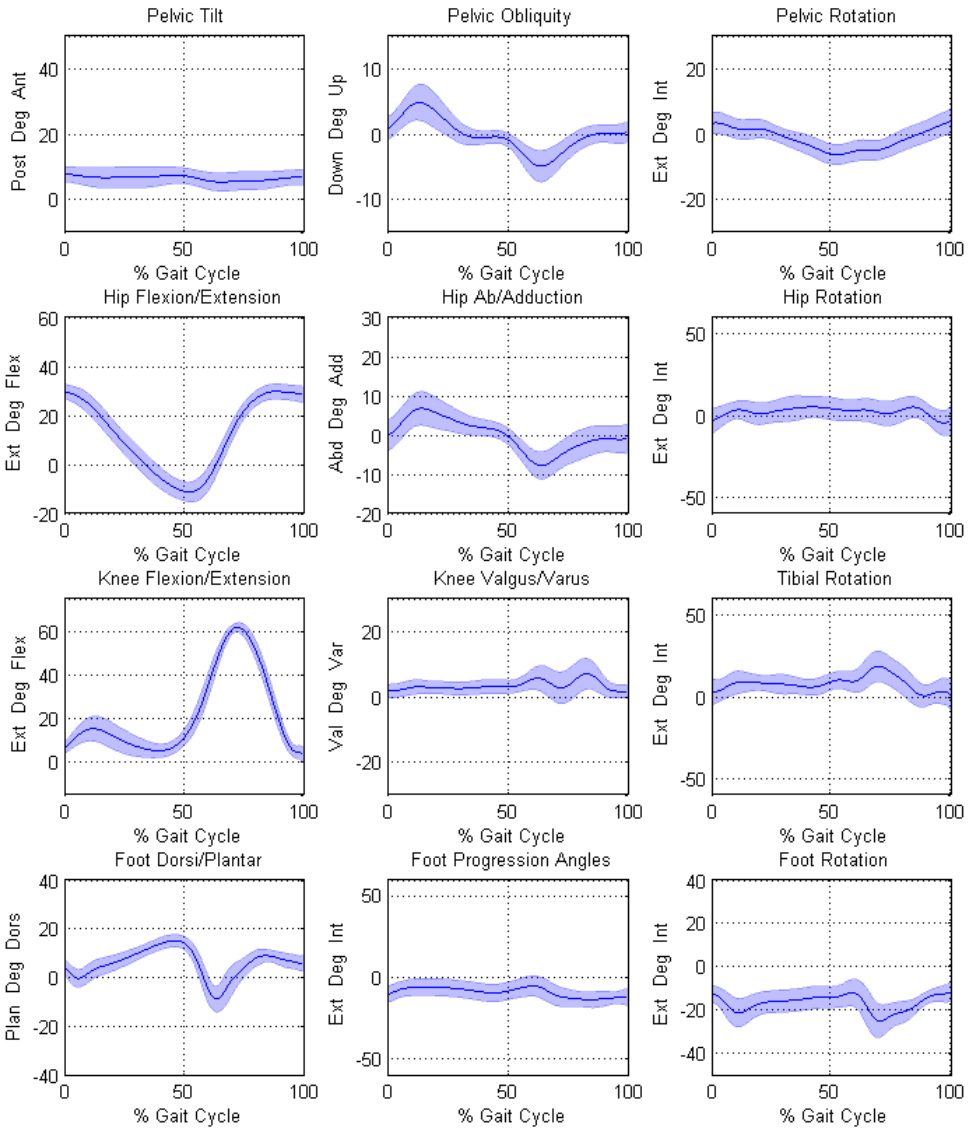

Figure 30: Visual3D plots of joint angle data for the right side.

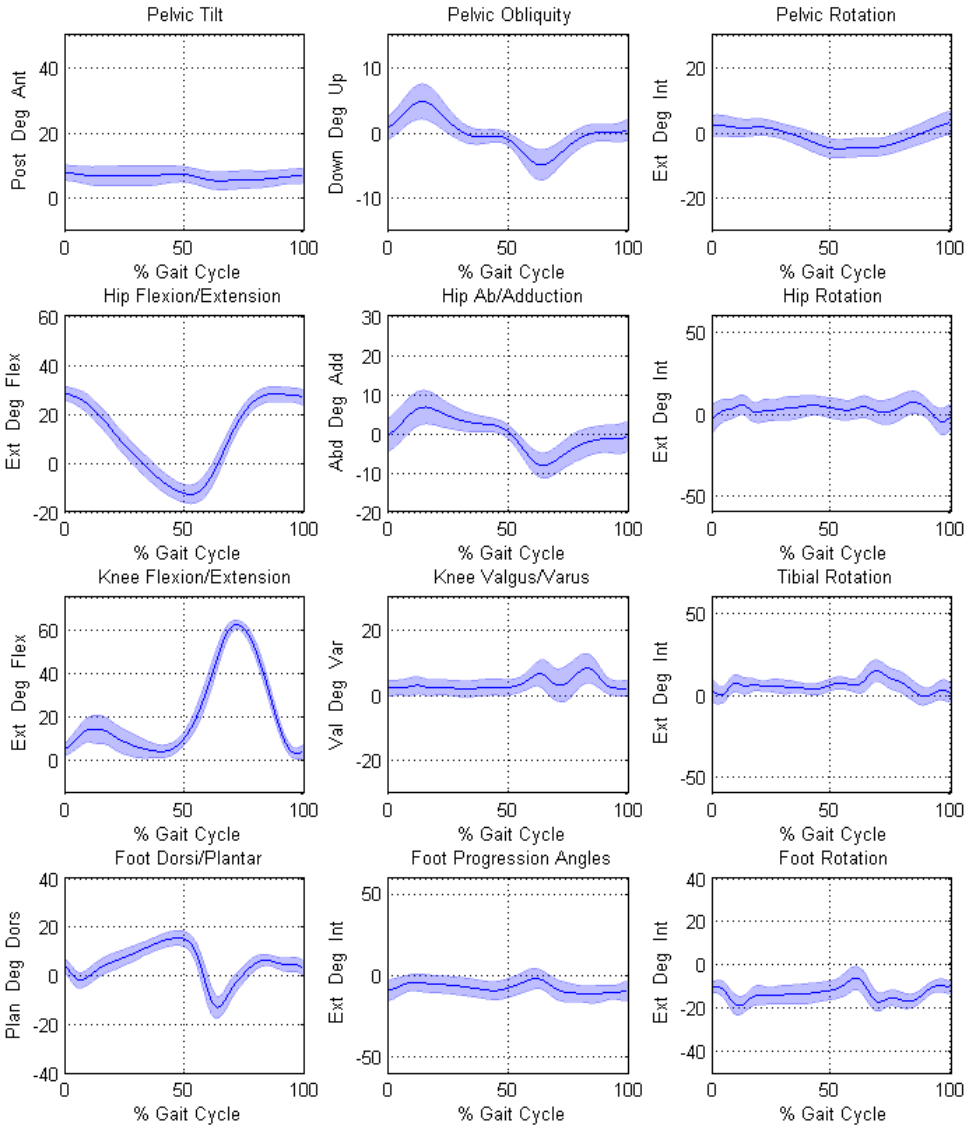

Figure 31: Nexus plots of joint angle data for the right side.

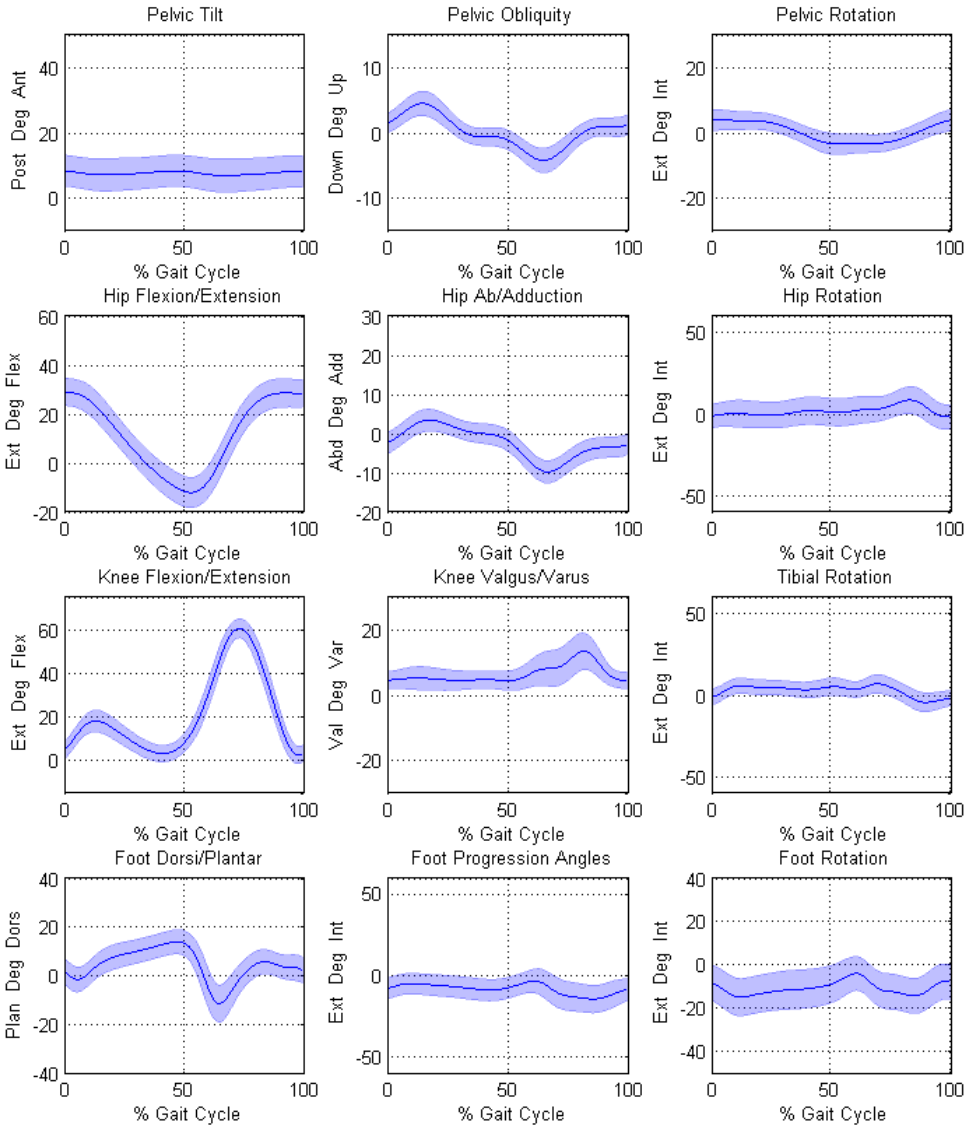

Figure 32: Clubfoot study [37] plots of joint angle data.

Appendix I

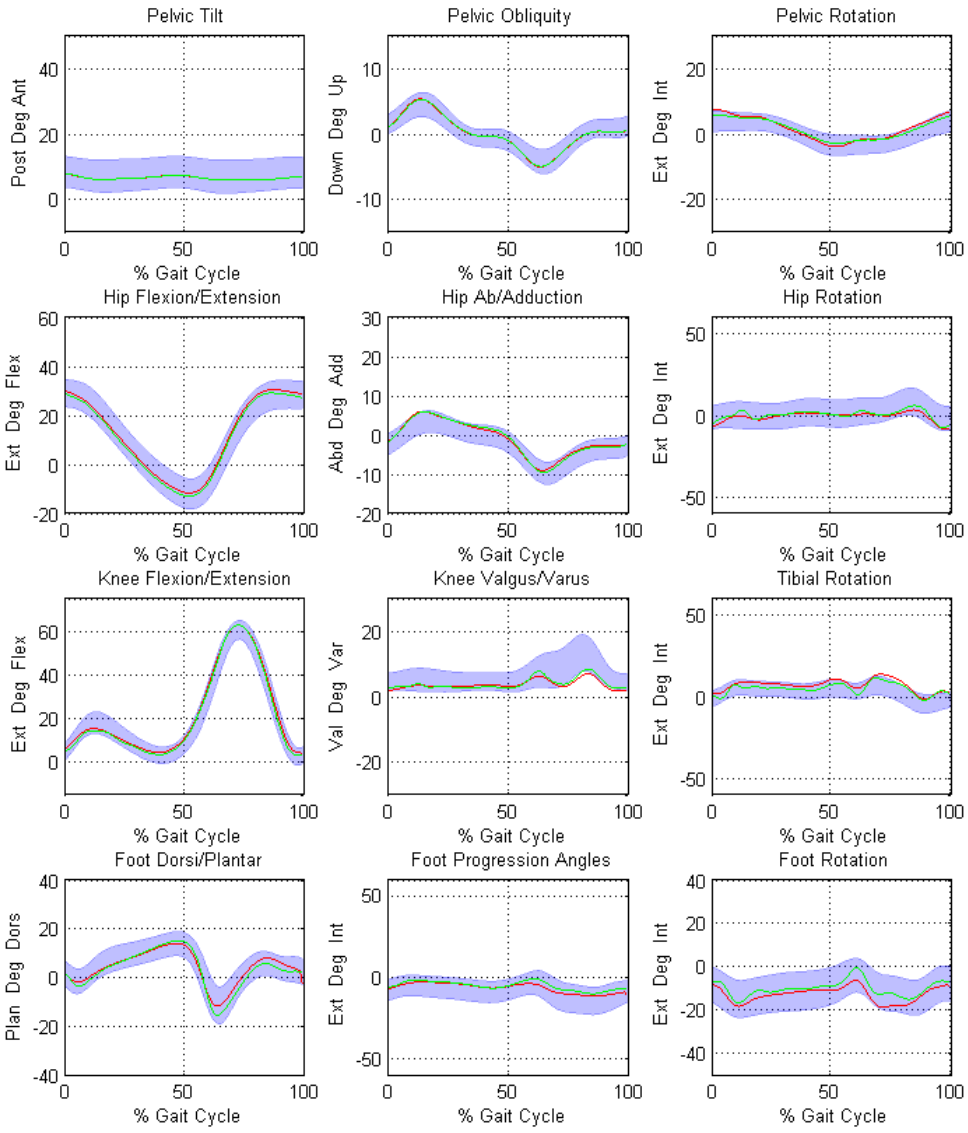

Figure 33: Left side - Clubfoot study standard deviation with Visual3D and Nexus means. Visual3D is red and Nexus is green.

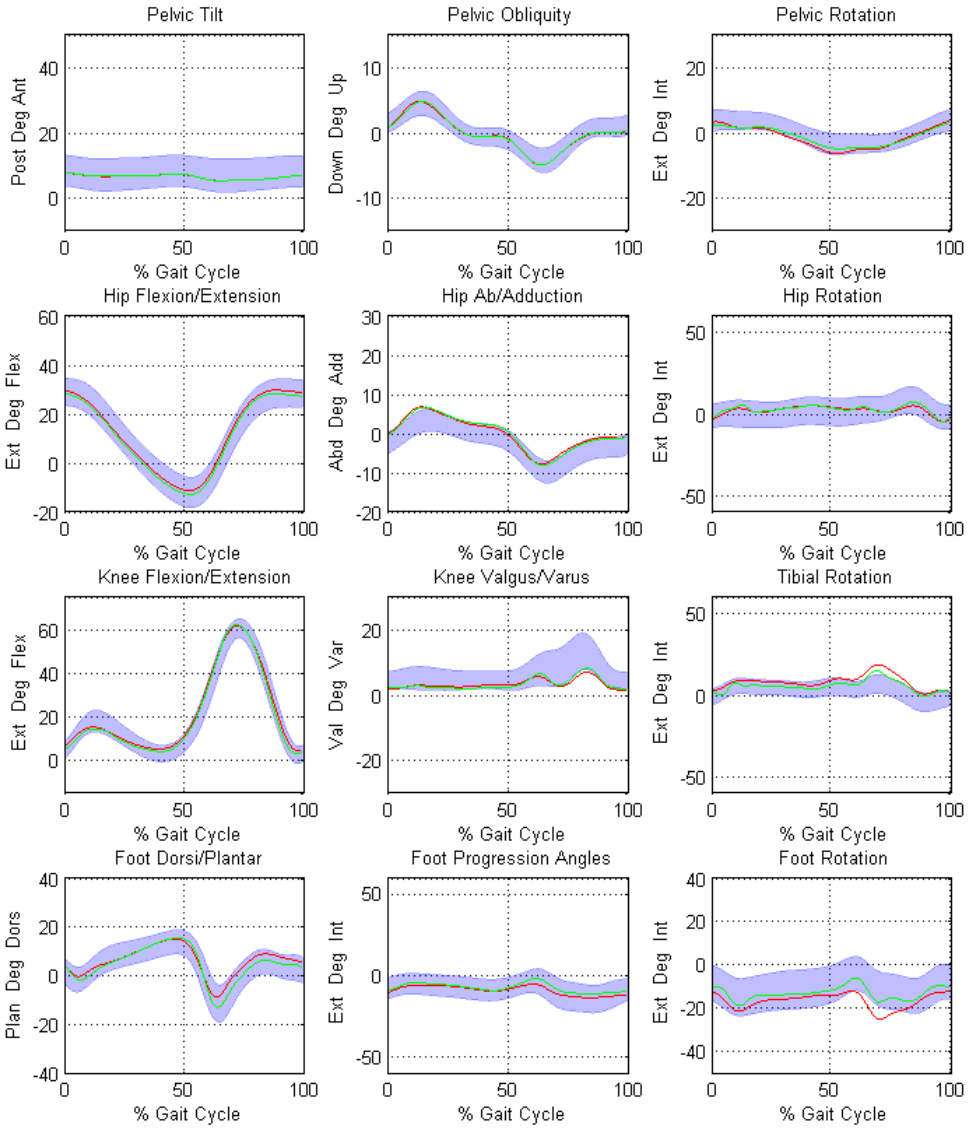

Figure 34: Right side - Clubfoot study standard deviation with Visual3D and Nexus means. Visual3D is red and Nexus is green.